Point-to-point responses to anonymous Reviewers

by Huan Yu, yuhuan@cug.edu.cn

We appreciate two anonymous referees for their insightful comments and careful examination of the manuscript. Below, we provide point-by-point responses to their comments and questions. The manuscript is revised accordingly.

Note: all the chemical formula data used in the manuscript can be accessed in "Global Change Research Data Publishing and Repository" via DOI:10.3974/geodb.2020.03.26.V1. This statement has been added to Data Availability in the finalized manuscript.

Reviewer comments 1

Review of Wan et al.:
The paper presents a thorough report on the observation of a new group of aerosol organic species in coastal new iodine particles. Further effort is directed towards identifying the nature of such organic compounds, and their different contribution to size-resolved aerosol samples. The paper is very detailed and very well written, although some language editing may be beneficial. This paper fits well within the scope of ACP. I would like to congratulate the authors for this novel iodine research and I recommend publication after the comments below are addressed:

- The authors argue the source of the reported organics is likely the same as for iodine emissions (i.e. algae exposed to the atmosphere at low tide). However, they should elaborate more about this since the results shown in the paper are not clear on this regard.

For instance, do they see similar levels of OC at high tide when no iodine emissions occur? At low tide, the instrument is between 40 and 200 m from the coastal line and the emission area. Can the authors comment on the effect of this distance on their measurements? Can they see gradual differences in aerosols composition as the water recedes?

Re:

Using our off-line techniques, only time-averaged mass concentration and chemical composition of OC were obtained for a period of three consecutive days. We thus cannot differentiate OC levels and composition between high tide and low tide. However, we have two indirect evidences to support that the OC observed in our manuscript was due to the photochemistry of low tide emissions: first, the online instruments NAIS and SMPS indicate indeed that number concentration of new particles was anti-correlated to tidal height, as show in our new Figure S2a below.

Second, during the three overcast non-NPF days from April 16 to 18, both total OC level and chemical composition in 10-18 nm size range were below or close to field blank.

As our future work, we are planning to conduct online measurement of chemical composition of clusters or nanoparticles at the site.

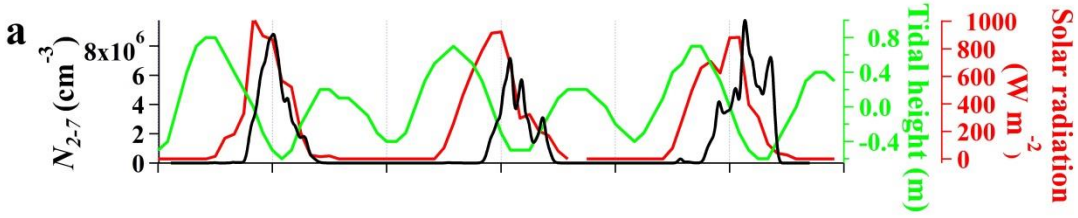

OC measured in iodine particles? Overall, the paper would benefit from some more detailed discussion on the possible sources of OC and the potential anthropogenic influence. This is important to be able to extrapolate their results to other iodine-rich coastal locations.

Re:
We add an aerial photo (Fig. S1a) to show the environment around the sampling site. Some description of the site is added in line 91-9 :

"*The sampling site (29°29′ N, 121°46′ E) is near a small fishing village without permanent residents in the coastline of East China Sea. It can be seen from the aerial photo (Figure S1a) that from the east to the west are the sea, intertidal zone, small paddy fields and the mountain.*"

In a new Fig S1b, we plot back trajectories during the I-NPF days from May 8 to 10, 2018.

The following discussion is added in line 156-161:

"*…strong I-NPF events were observed almost every sunny day in April and May, which was the growth and farming season of seaweed. HYSPLIT Back-trajectories analysis (Draxler and Rolph, 2010) shows that air masses moved from East China Sea to the sampling site during the I-NPF days from May 8 to 10, 2018 (Figure S1b). Sea breeze was also expected to flow from the sea to the site in the daytime when the I-NPF events occurred.*"

In line 358-363:

"*Obviously, $C_{18,30}H_hO_oN_n$ and $C_{20,24,28,33}H_hO_o$ formulas cannot be attributed to continental terpene emission or anthropogenic aromatic emissions. Sporadic spikes of*

10-18 nm particles that can be an indication of cooking and traffic emissions were not seen in the PNSD spectrum, because such human activities were rare around the site during the sampling period. We thus also exclude the possibility of cooking and traffic emissions."

In summary, considering the unique OC chemical formulas (i.e. $C_{18,30}H_hO_oN_n$ and $C_{20,24,28,33}H_hO_o$) and their co-presence with iodine in the new particles, we suggest the results in our location can be extrapolated to other iodine-rich coastal locations, as long as iodine-NPF could be observed.

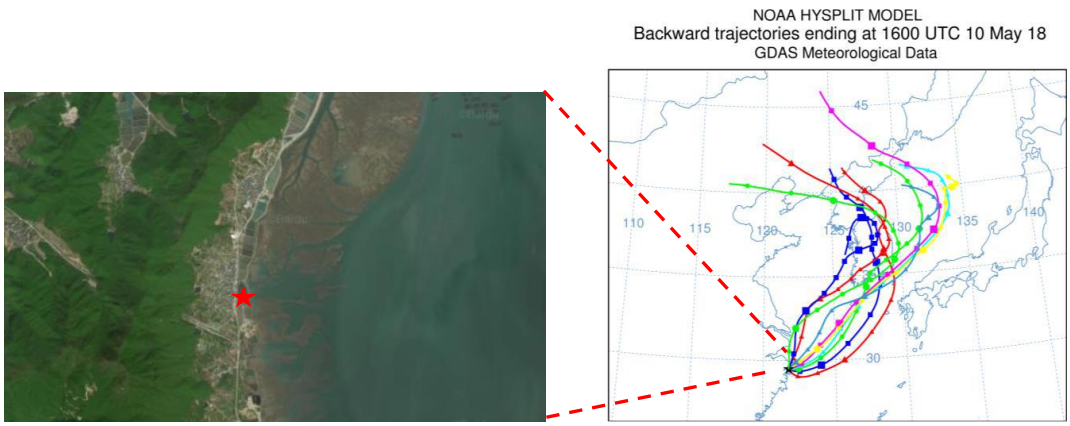

Figure S1. (a) The observation site, indicated as a red star, in an aerial photograph. Photo source: Baidu Map. (b) 72-hour air mass back trajectories ending at 100 m above ground level at the observation site computed by HYSPLIT model during the I-NPF events from May 8 to 10, 2018.

- Line 49, beginning of paragraph. It would be useful for the reader to clarify that organic iodine is not the main source of the iodine oxide precursors that lead to the formation of I-NPF. This was shown in the past for coastal regions: A. Saiz-Lopez and J. M. C. Plane, Novel iodine chemistry in the marine boundary layer. Geophys. Res. Lett. 31, L04112 (2004). and for opean ocean conditions: A. S. Mahajan et al., Measurement and modelling of tropospheric reactive halogen species over the tropical Atlantic Ocean. Atmos. Chem. Phys. 10, 4611-4624 (2010). A. S. Mahajan et al., Latitudinal distribution of reactive iodine in the Eastern Pacific and its link to open ocean sources, Atmospheric Chemistry and Physics, 12, 11609-11617 (2012).

Re:
The sentence is revised and the references are cited in line 51-57:
"*Unlike the deep understanding of continental HOMs, little is known about the role of organics in the NPF in coastal or open ocean atmosphere. The current state of knowledge is that the photolysis of molecular iodine (I_2) or iodomethane is the source of iodine oxides or oxoacids, the self-clustering of which could initiate NPF events with particle number concentration sometimes exceeding 10^6 cm^{-3} (O'Dowd et al., 2002; Saiz-Lopez and Plane, 2004; Burkholder et al., 2004; Mahajan et al., 2010,*

2012; Sipilä et al., 2016; Stevanović et al., 2019; Kumar et al., 2018)."

- Final comment. I would suggest to add a sentence to the Conclusions about the potential relevance of extrapolating the results of this location to other coastal locations, based on the questions above.

Re:
The following statement is added in the conclusion part line 543-548:
"*This article reveals a new group of important organic compounds involved in this process. It is most likely that their precursors are emitted mutually with iodine from either direct exposure of coastal biota to the atmosphere or biological-active sea surface. If this is true, we suggest the results in our location can be extrapolated to other iodine-rich coastal locations, as long as iodine-NPF can be observed.*"

Reviewer comments 2

Review of Wan et al., 2020:
This paper contains reports on the multitude of organic compounds present in size segregated aerosol samples at a coastal location where frequent new particle formation (NPF) was observed, as measured by a powerful off-line mass spectrometric technique. Iodine-NPF events are identified (I-NPF) and these are linked to aerosol chemical composition during periods with three days of consecutive I-NPF days. These are compared with similar data for C-NPF days. The potential sources are discussed, and volatilities of these compounds as calculated by a group contribution method are presented and discussed with a view to linking these compounds to new particle growth. The paper is well within the remit of ACP and contains a very valuable dataset in a field where not much is yet known, however, I find issues with the authors' definition of I-NPF, and the discussion of calculated vapour pressures could do with some extension as there are many uncertainties with these calculations not discussed. I recommend publication after the following issues are addressed.

General comments:
- In **section 3.1** the authors present 10-56 nm particle phase composition in 72 hour aerosol samples through 3 consecutive NPF days of two different categories (iodine-induced NPF, or *I-NPF*, & continental regional NPF, or *C-NPF*), identified from size-distribution measurements. It is evident from the size distributions that these NPF days *are* very dissimilar, and the evolution of the size distribution is markedly similar to prior reports of iodine-nucleation (such as Sipilä et al., 2016), however, the authors state that an elevation to the mass concentration of iodine in 10-56 nm aerosol samples during the I-NPF days is clear indication that NPF was linked to iodine nucleation. I would strongly argue this is not a clear indication a nucleation process involving iodine vapours, as aerosol mass between 10-56 nm is not an indicator of what process produces particles at ~1.7 nm. I would urge the authors to back this claim up with reference to similar reports of iodine driven nucleation under conditions that produce either similar particle composition or similar size distributions. HSO4- concentrations are still an order of magnitude higher than I- concentrations in 10-18 nm particles on I-NPF days. If there is there any evidence within the data that nucleation processes are not dominated, for example, by sulphuric acid processes, this would strengthen this section greatly.

Re:
In the revised manuscript we list four facts following the suggestions of the reviewer. In line 154-173, the revised part reads as follows:

"Although our offline technique did not allow us to probe nucleating cluster composition at ~1.7 nm, four facts from our observation support that the NPF events from May 9 to 11 were initiated by iodine nucleation. First, strong I-NPF events were

observed almost every sunny day in April and May, which was the growth and farming season of seaweed. HYSPLIT Back-trajectories analysis (Draxler and Rolph, 2010) shows that air masses moved from East China Sea to the sampling site during the I-NPF days from May 8 to 10, 2018 (Figure S1b). Sea breeze was also expected to flow from the sea to the site in the daytime when the I-NPF events occurred. Second, the evolution of PNSD from May 9 to 11 was not like banana-shape C-NPF observed on the winter days, but was markedly similar to prior reports of iodine-nucleation at European coastal sites (Mäkelä et al., 2002; Sipilä et al., 2016). Third, the production of 2-7 nm particles (N_{2-7}) during the C-NPFs followed a nearly identical variation with solar radiation (Figure S2c), which is an indication that the C-NPFs was initiated by OH and H_2SO_4 production dictated by solar radiation. However, this was not observed during the I-NPF events, instead, N_{2-7} was anti-correlated to tidal height in the daytime (Figure S2a). Fourth, probably the most important, mean total I in 10-56 nm particles during the I-NPF days (13.5 ng m^{-3}, Table 1) was 67 and 36 times higher than those during the C-NPF days (0.2 ng m^{-3}) and non-event days (0.37 ng m^{-3}). In the same size range, mean HSO_4^- concentration (0.2 μg m^{-3}) during the I-NPF days was lower than that during the C-NPF days (0.5 μg m^{-3}).”

Another comparison with previous iodine studies in terms of chemical composition is added in line 182-185:

…Our result is qualitatively consistent with previous measurements showing that nucleation mode particles initiated by iodine were composed of a remarkable fraction of organics and sulfate (Mäkelä et al., 2002; Vaattovaara et al., 2006).”

The time series of N_{2-7}, tidal height and solar radiation are added to Figure S2.

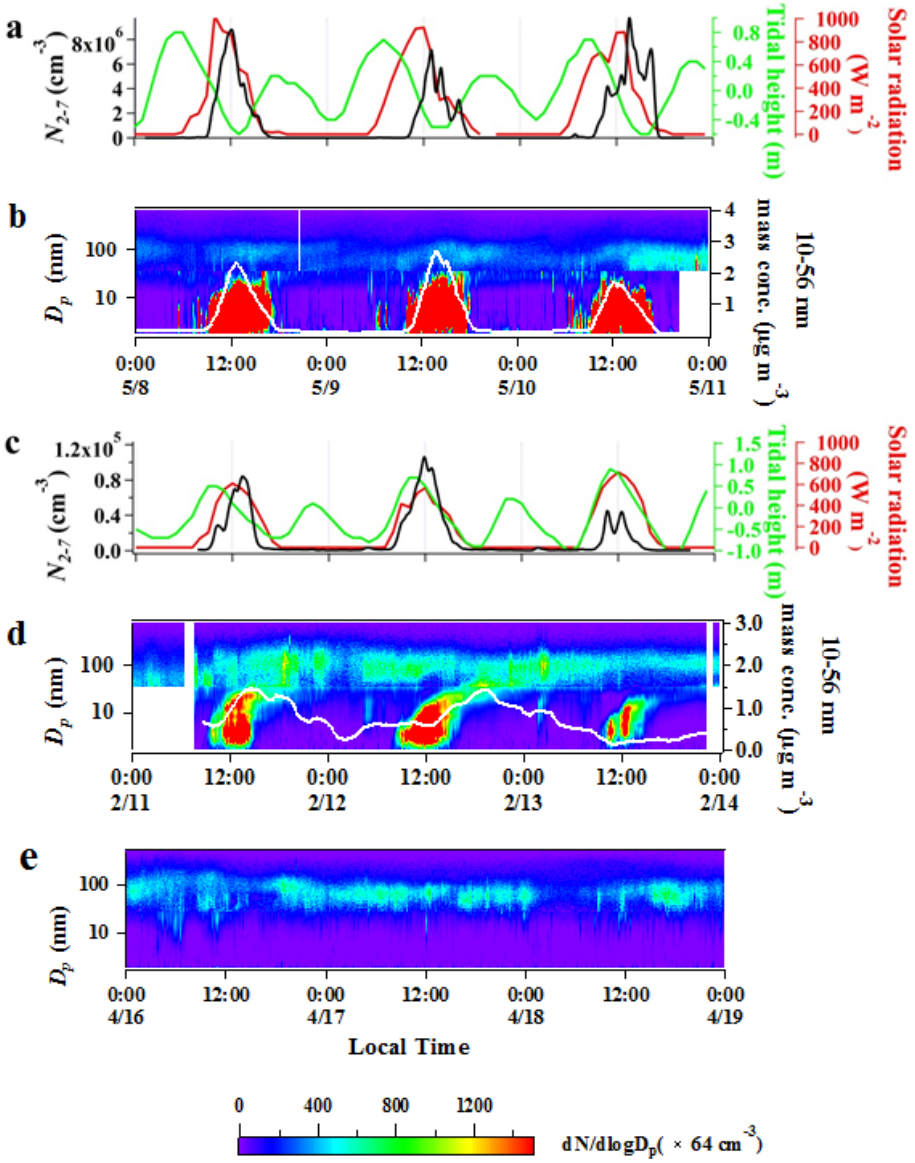

Figure S2. (a), (c) Number concentration of 2-7 nm particles ($N_{2\text{-}7}$), tidal height and solar radiation intensity during the Iodine-initiated NPF (I-NPF) days from May 9 to 11 and the continental regional NPF (C-NPF) days from February 11 to 13. Particle number size distribution during (b) I-NPF days from May 9 to 11, (d) C-NPF days from February 11 to 13 and (e) non-NPF days from April 16 to 18.

- It would be very useful to mention the magnitude of the effect of these NPF events to aerosol mass in the relevant size ranges – coming up with an exact number is a rather uncertain process, but a simple alternative would be a plot showing the time evolution of size-segregated aerosol mass as currently there is no indication of how much of the aerosol mass is actually arising from NPF.

Re:
The time series of mass concentration of 10-56 nm particles was estimated from the PNSD data by assuming a particle density of 1.5 g cm^{-3}. The time series was added to Figure S2.

The inserted sentences in line 174-182 read as

"By assuming nanometer sized particles are spherical with a density of 1.5 g cm^{-3}, we estimate from the PNSD data that aerosol mass in the 10-56 nm size range was enhanced by 3.0 and 1.3 μg m^{-3} at most by the selected I-NPF and C-NPF events (Figure S2b and S2d). The fraction of organic mass (OM) in the aerosol mass can be further calculated from $(1.5\times m_{TOC})/(m_{Total\ I} + m_{HSO4^-} + 1.5\times m_{TOC})\times 100\%$ by assuming an OM/TOC ratio of 1.5. The result shows that mass fractions of OM are 95%, 87% and 68%, respectively, in the size bins 10-18 nm, 18-32 nm and 32-56 nm during the I-NPF days. Therefore, organic compounds dominate the aerosol mass in the 10-56 nm new particles during the I-NPF days and were critical for I-NPF to contribute to CCN."

- Recent chamber results utilising EESI-ToF-MS would indicate that oligermisation processes in the particle phase can produce a diverse range of compounds (Pospisilova et al., 2020), as well as particle phase processes producing organosulphates (Mutzel et al., 2015), formation of ester hydroperoxides (Zhao et al., 2018) etc. I would consider how such mechanisms may affect your proposed formation mechanisms, and further your estimations of volatility - if some of these compounds arise from particle-phase oligomerisation, does this change the conclusions of the paper? I would like to echo reviewer #1 here and suggest an extension of the discussion so the results can be more easily extrapolated to other coastal regions.

Re:
According to the paper by Pospisilova et al., 2020 and others, both monomers (C5–C10) and dimers (C15–C20) are evident in chamber organic aerosols produced by alpha-pinene ozonolysis. Moreover, the mass spectrum is dominated by monomer signals. We didn't see such monomer-dimer distribution pattern in our mass spectrum for either $C_{18,30}H_hO_oN_n$ or $C_{20,24,28,33}H_hO_o$ formulas.

Multifunctional organic peroxides, such as αAAHPs, may comprise an important but unresolved fraction of SOA (Zhao et al. 2018 a,b). These studies also

demonstrated that organic peroxides may undergo fast hydrolysis or decomposition to end products containing carboxyl, carbonyl or hydroxyl groups. A basic assumption in our study is the formulas we observed are end products. Our volatility estimation thus considered only end products containing $–ONO_2$, –OH, –C=O, $–NH_2$ and -COOH groups. The formation of those intermediates like αAAHPs in the gas phase and air-water interface is possible, but not measurable by our methods.

However, the missing information about possible intermediates will not change the conclusion of our manuscript, that is, the addition of $–ONO_2$, –OH, –C=O , and -COOH groups to biogenic precursors reduced the volatility of precursors by 2~7 orders of magnitude and the end products containing $–ONO_2$, –OH, –C=O , $–NH_2$, -COOH groups fall into the range of ELVOC and ULVOC. In fact, the formation of low volatility intermediates like αAAHPs may further enhance the partitioning of organic products to particle phase.

Organosulfate accounted for only ~10% of ESI- signals in 10-18 nm particles. Their possible formation in the gas or particle phase is beyond the focus of our manuscript. We didn't discuss their formation mechanism and volatility in the manuscript.

We add the following statement in line 325-329:

"Monomer-dimer distribution pattern that can arise from particle-phase oligomerisation (Pospisilova et al., 2020) was not observed for these formulas in the mass spectra. We also assume that $C_{18,30}H_hO_oN_n$ and $C_{20,24,28,33}H_hO_o$ are not labile intermediates like ester hydroperoxides that may undergo fast decomposition in the particles or during the sample preparation process (Zhao et al. 2018 a,b)."

- The estimation of volatilities through SIMPOL has some associated uncertainties, and, at least in the case of HOMs, estimations of volatility can vary by several orders of magnitude when compared with other methods (see Figure 8 of Peräkylä et al., 2019). This should be a point of discussion as it may affect the outcomes of the paper.

Re:
The volatility of VOC oxidation products can be assessed with numerous existing parameterizations, which require either exact functional groups making up a molecule or only the molecular formula. Their estimation can be consistent with each other quite well or vary by up to several orders of magnitude. At this moment, we cannot declare which is better than others. For example, the equation given by the Peräkylä et al., 2019 method may only hold for SVOC and LVOC range, because the gas-particle partitioning behavior of the compounds outside the SVOC and LVOC range cannot be measured easily by the Peräkylä et al., 2019 method.

But this will not change the conclusion drawn in the manuscript, that is, the addition of $–ONO_2$, –OH, –C=O , and -COOH groups reduces the volatility of precursors greatly and thus make their oxidation products condensable onto new particles during the I-NPF event days.

In line 485-489 we add

"*It should be noted that the volatility of VOC oxidation products can be assessed with numerous existing parameterizations, which require either exact functional groups or only the molecular formula (Peräkylä et al., 2019). Their estimation can vary by up to several orders of magnitude. But this will not change the conclusion drawn here.*"

Specific comments:

Line 22 and throughout: Change "organics" to "organic compounds".

Re: corrected.

Line 43: "Highly oxygenated (multifunctional) organic molecules" is a more correct term for these than "highly-oxidised" (see Bianchi et al., 2019)

Re: corrected.

Line 44: If you're using Extremely Low Volatility here to refer to molecules that fall into the volatility class $C^*(300K)\ 3\cdot10^{-9} < C^*(300K) < 3\cdot10^{-5}$ µg m^{-3}, then it is worth note that by current classification of HOMs as discussed in Bianchi et al., 2019, HOMs fall across many of these volatility classes. As you refer to nucleation on line 47, I would consider revising this statement as it is currently thought that only ULVOC (as defined by Schervish & Donahue, 2019; Simon et al., 2020) are capable of undergoing pure biogenic nucleation. I would include this also in your discussion of section 3.3.3, as many of your compounds fall into this volatility class and this could make a valuable addition to this discussion.

Re:

Now we delete "extreme" from line 45. What we want to say here is HOMs with low volatility contributed to both nucleation/growth and SOA formation. The statement reads as follows:

"*..Recent laboratory and field studies have identified a group of highly oxygenated multifunctional organic molecules (HOMs) with high O/C ratios and low volatility… These HOMs play an important role in particle nucleation and growth of continental NPF, as well as in the formation of secondary organic aerosols.*"

In section 3.3.3 we revise the following statements:

"*As we can see in Table S4, C* of the 49 formulas fall into the range of ELVOC (3 × 10^{-9} - 3 × 10^{-5} µg m^{-3}) and even ULVOC (ultra-low volatility organic compound, <3 × 10^{-9} µg m^{-3}), while C* of their precursors are in the range of SVOC (0.3-300 µg m^{-3})*

or LVOC (3×10^{-5}-0.3 μg m^{-3}). The addition of functional groups reduces the volatility of precursors by 2~7 orders of magnitude and thus make their oxidation products condensable onto new particles during the I-NPF event days. According to the definition of Schervish and Donahue, 2019 and Simon et al., 2020, ULVOC can even drive pure biogenic nucleation. Therefore, the analysis of precursor-product volatility partly supports our hypothesis about the molecular identity and formation mechanism of the formulas detected in 10-18 nm particles."

Line 46-47: Given the nature of the paper, it may also be worth mentioning recent work discussing formation of HOMs from chlorine oxidation also (Wang et al., 2020).

Re:
We add chlorine atom and cite the paper of Wang et al., 2020 in line 48.

Line 89: It would be nice if you provided more detail here for those unfamiliar with I-NPF. How does the evolution of the size distribution differ from conventional "banana-plot" NPF? This definition feels very arbitrary. Is there also any air-mass data that can support the assignment of "I-NPF"? It would be very beneficial to have a steadfast criteria that separates the two.

Re:
Please see our response to your earlier comment. We present four facts, including air mass back trajectory analysis, to support the definition of I-NPF in line 154-173, Section 3.1

Table 1: Consider using the same units (μg m^{-3}) for all quantities.
Re:
Change ng m^{-3} to μg m^{-3}

Line 208-209: "The formula number of the least common CHN^+ group is only 46". Do you mean CHN^+ is the least common group?
Re:
Yes, CHN+ is the least common group.

Line 214-216: Is there any evidence for the role of amines in iodine nucleation? A reference to this would be informative here, otherwise it is of little relevance given the section discusses iodine nucleation
Re:
There is no evidence or reference for the role of amines in iodine nucleation. However, generally speaking, basic amines are expected to stabilize H_2SO_4-H_2O cluster in atmospheric NPF. People may be curious if amines can be present in our particles in such an location where marine organism can be a significant source of amine emission. So we just want to report here that amines contributed a negligible fraction

to new particles in our case.

Line 301-303: It is not evident to me that these spectra indicate oxidation products of continental terpene emissions, the peaks at 9-10, 13-15 and 18-20 carbon numbers that would typically be expected of these products are not present. This point could do with expanding.

Re:

It can be clearly seen Figure 3d and Figure 2c that CHO^- formulas in the 180-560 nm particles are trimodal with maximum intensity around C_9, C_{13}-C_{16} and C_{20}, while $CHON^-$ are bimodal around C_{10} and C_{15}.

Technical corrections:

Line 44: High O:C ratio**s** (rather than “ratio”)

Line 72-73: Change "Studies investigating coastal organic aerosols have been rarely" to "...aerosols are rare"

Line 80: Missing hyphen in FT-ICR-MS

Line 86: Space between 200 and m

Figure S1: I would urge the authors to consider using a colour scale that does not "cap out" at 1,500x64 cm^{-3} as this disingenuously misrepresents the I-NPF event.

Line 149: Should this read “Nanometer *sized* new particles”?

Figure S2 and throughout: Dalton is not a unit of mass/charge.

Line 222: Should this read (free) troposphere?

Line 253: change to “**a** relatively high unsaturation degree”

Re:

We appreciate the reviewer for his/her care examination of the manuscript. All problems are now solved following the comments above.

Probing key organic substances driving new particle growth initiated by iodine nucleation in coastal atmosphere

Yibei Wan,[1] Xiangpeng Huang,[2] Bin Jiang,[3] Binyu Kuang,[4] Manfei Lin,[4] Deming Xia[5], Yuhong Liao,[3] Jingwen Chen,[5] Jianzhen Yu,[4] and Huan Yu[1]

[1] Department of Atmospheric Science, School of Environmental Studies, China University of Geosciences, Wuhan, 430074, China

[2] School of Environmental Science and Engineering, Nanjing University of Information Science and Technology, Nanjing, 210044, China

[3] Guangzhou Institute of Geochemistry, Chinese Academy of Sciences, Guangzhou 510640, China

[4] Department of Chemistry, Hong Kong University of Science & Technology, Clear Water Bay, Kowloon, Hong Kong, China

[5] School of Environmental Science and Technology, Dalian University of Technology, Dalian 116024, China

Corresponding author: H. Yu (yuhuan@cug.edu.cn)

Graphic abstract

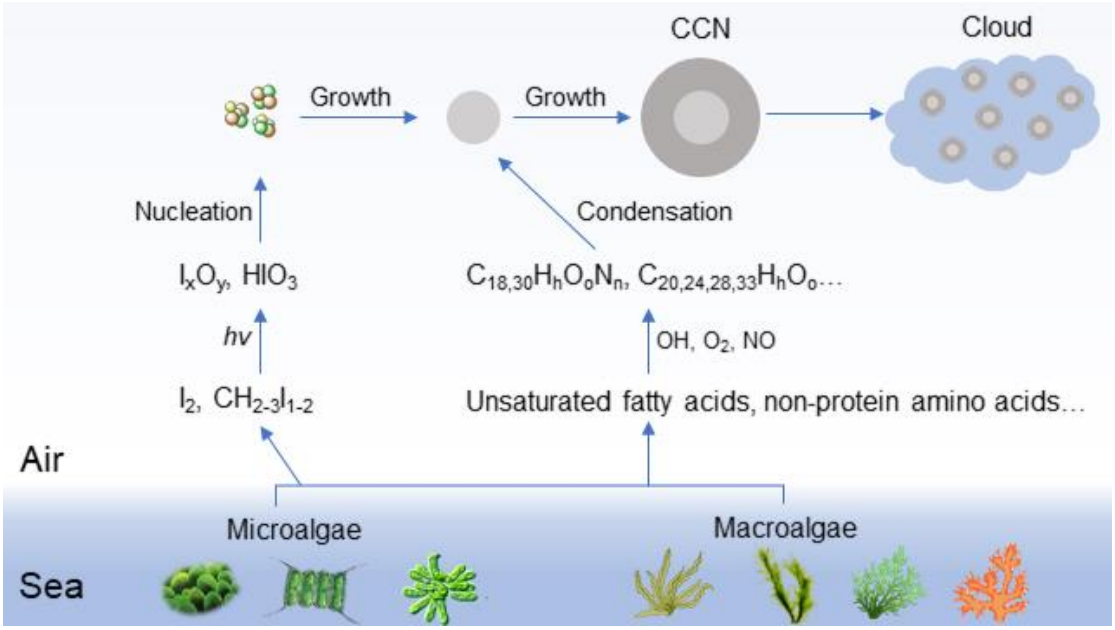

ABSTRACT

Unlike the deep understanding of highly oxygenated organic molecules (HOMs) driving continental new particle formation (NPF), little is known about the organic compounds involved in coastal and open ocean NPF. On the coastline of China we observed intense coastal NPF events initiated by iodine nucleation, but particle growth to cloud condensation nuclei (CCN) sizes was dominated by organic compounds. This article revealed a new group of $C_{18,30}H_hO_oN_n$ and $C_{20,24,28,33}H_hO_o$ compounds with specific double bond equivalents and oxygen atom numbers in sub-20 nm coastal iodine new particles by using ultrahigh resolution Fourier transform-ion cyclotron resonance mass spectrometry (FT-ICR-MS). We proposed these compounds are oxygenated or nitrated products of long chain unsaturated fatty acids, fatty alcohols, non-protein amino acids or amino alcohols emitted mutually with iodine from coastal biota or biological-active sea surface. Group contribution method estimated that the addition of $–ONO_2$, –OH and –C=O groups to the precursors reduced their volatility of by 2~7 orders of magnitude and thus made their products condensable onto iodine new particles in the coastal atmosphere. Non-target MS analysis also provided a list of 440

formulas of iodinated organic compounds in size-resolved aerosol samples during the iodine NPF days, which facilitates the understanding of unknown aerosol chemistry of iodine.

1. INTRODUCTION

Atmospheric new particle formation (NPF) contributes over half of global cloud condensation nuclei (CCN) (Merikanto et al., 2009) and thus influences cloud properties and Earth's radiation budget (Metzger et al., 2010). By deploying high resolution Chemical Ionization Mass spectrometer, recent laboratory and field studies have identified a group of highly oxygenated multifunctional organic molecules (HOMs) with high O/C ratios and low volatility from the reactions of volatile organic compounds (VOCs) such as monoterpenes (Ehn et al., 2014), Sesquiterpenes (Richters et al., 2016) and alkene (Mentel et al., 2015) with hydroxyl radical (OH), ozone (O_3), nitrate radicals (NO_3) and chlorine atom (Wang et al., 2020). These HOMs play an important role in particle nucleation and growth of continental NPF, as well as in the formation of secondary organic aerosols.

Unlike the deep understanding of continental HOMs, little is known about the role of organic compounds in the NPF in coastal or open ocean atmosphere. The current state of knowledge is that the photolysis of molecular iodine (I_2) or iodomethane is the source of iodine oxides or oxoacids, the self-clustering of which could initiate NPF events with particle number concentration sometimes exceeding 10^6 cm^{-3} (O'Dowd et al., 2002; Saiz-Lopez and Plane, 2004; Burkholder et al., 2004; Mahajan et al., 2010, 2012; Sipilä et al., 2016; Stevanović et al., 2019; Kumar et al., 2018). But it is unknown if other species are needed to drive the growth of iodine clusters to CCN sizes in coastal or open ocean atmosphere (Saiz-Lopez et al., 2012). Iodine-induced NPF (I-NPF) events were mostly reported in European coastlines (Yoon et al., 2006; Mahajan et al., 2010) and polar regions (Allan et al., 2015; Roscoe et al., 2015; Dall Ósto et al., 2018). In 2019 we provided evidences of I-NPF in the southeast coastline of China, based on particle number size distribution and iodine measurements (Yu et al., 2019). The focus

of that paper (Yu et al., 2019) is, however, the speciation of organic iodine compounds in size-segregated aerosol samples. Moreover, the use of relatively low resolution Time-of-Flight (TOF) mass analyzer and *in vitro* signal amplification approach in that paper did not allow the detection of the majority of non-aromatic organic iodine compounds. Organic iodine remains to be the most significant unknown in aerosol iodine chemistry at present (Saiz-Lopez et al., 2012).

Fourier Transform Ion Cyclotron Resonance (FT-ICR) coupled with soft ionization techniques such as electrospray ionization (ESI) and ambient pressure chemical ionization (APCI) allows characterization of complex organic mixtures at the molecular level due to its ultra-high resolution and mass accuracy (Pratt and Prather, 2012). This technique has been used to examine molecular composition of organic aerosols (Schum et al., 2018; An et al., 2019; Zuth et al., 2018; Daellenbach et al., 2018; Xie et al., 2020) and cloud water (Zhao et al., 2013; Bianco et al., 2018). Studies investigating coastal organic aerosols have been rare. Virtually no study reported the characterization of organic compounds driving the growth of coastal or open ocean new particles.

In this study, comprehensive chemical composition analyses were conducted on the size-segregated aerosol samples down to 10 nm, collected by 13-stage nano-MOUDI (nano-micro orifice uniform deposit impactor) during the intense I-NPF days at a coastal site of China. Relative abundances of HSO_4^-, total iodine and total organic carbon (TOC) in 10-56 nm particles were compared between the I-NPF days and conventional continental NPF (C-NPF) days. In particular, using ultra-high resolution FT-ICR-MS, we conducted a non-target analysis of particle-phase organic compounds to explore their molecular identity, formation mechanism and the role in new particle growth in the coastal atmosphere.

2. METHDOLOGY

2.1. Sampling collection

The sampling site (29°29′ N, 121°46′ E) is near a small fishing village without permanent residents in the coastline of East China Sea. It can be seen from the aerial photo (Figure S1a) that from the east to the west are the sea, intertidal zone, small paddy fields and the mountain. The sampling site is about 40 and 200 m away from at high tide and low tide, respectively. The classification of I-NPF event, C-NPF event or non-NPF was based on particle number size distributions (PNSD) between 2 and 750 nm monitored from January to May 2018 by a scanning mobility particle spectrometer (SMPS; TSI DMA3081 and CPC3775; scanning range: 40-750 nm) and a neutral cluster air ion spectrometer (NAIS; scanning range: 2-42 nm). A nano-MOUDI sampling scheme was implemented according to the PNSD measurement. One set of nano-MOUDI samples was collected during the C-NPF days from February 11 to 13; a second set was collected during overcast non-NPF days from April 16 to 18; a third set was collected during the I-NPF days from May 9 to 11. The PNSD during the 3 periods are shown in Figure S2. Each set of nano-MOUDI samples was collected continuously for 72 hours, during which NPF occurred on a daily basis, so that particle chemical composition of different event types can be obtained from offline analyses. Aluminum foil filters were used as sampling substrate to avoid the adsorption of gaseous species. For each set of nano-MOUDI samples, two nano-MOUDIs were placed side by side to collect 10-100 nm particles (on stages 10-13; other stages were silicon greased) and 100 nm-18 μm particles (on stages 1-9) separately, in order to reduce potential positive particle-bounce artifacts. Three additional sets of blank samples were collected by placing a high efficiency particulate air (HEPA) filter at the gas inlet of nano-MOUDI. Detailed information on aerosol sample collection could be found in Yu et al. (2019).

2.2. Sample preparation and analysis

Half of each filter was transferred into a 20 mL tapered plastic centrifuge tube, added 10 mL mixed solvent (1:1 v/v water and methanol; LCMS grade). The mixture was sonicated for 40 min and filtered by a 0.2 μm PTFE membrane syringe filter. The filtrate was evaporated to almost dryness in a rotary evaporator below 40 ℃ and subsequently redissolved in 0.5 mL water. After being centrifuged for 30 min at 12,000 rpm, the supernatant was collected for total iodine (I) analysis by Agilent 7500a ICP-MS (Agilent Technologies, Santa Clara, CA, USA) and HSO_4^- analysis by UPLC-ESI-Q-TOF-MS. The measurements of HSO_4^- and total I were elaborated in our previous article Yu et al. 2019. Another half of each filter was extracted in the same way but used for TOC analysis by a TOC analyzer (Model TOC-5000A, Shimadzu, Japan) and non-target MS analysis of organic compounds (OC) by ESI-FT-ICR-MS (SolariX XR 9.4T instrument, Bruker Daltonics, Coventry, UK). Samples were infused by a syringe pump and analyzed in both positive (ESI+) and negative (ESI-) modes. ESI-FT-ICR MS operation conditions are included in Supplement Material. Field blank sample extracts were analyzed following the same procedure.

2.3. FT-ICR MS data processing

A resolving power ($m/\Delta m_{50\%}$) 550,000 at m/z 300 of our FT-ICR-MS allows the determination of possible formulas for singly charged molecular ions. Only m/z values between 150-1000 Da that satisfies signal/noise (S/N) ratio > 10 were considered. For each m/z value, several scientific rules were applied to calculate a reasonable elemental formula of natural organic molecule: the general formula is $C_{1\text{-}50}H_{1\text{-}100}O_{0\text{-}50}N_{0\text{-}10}I_{0\text{-}3}$ in the ESI+ mode; elemental ratios H/C, O/C, and N/C are limited to 0.3-3, 0-3 and 0-1.3, respectively. The general formula is $C_{1\text{-}50}H_{1\text{-}100}O_{1\text{-}50}N_{0\text{-}5}S_{0\text{-}2}I_{0\text{-}3}$ in the ESI- mode; elemental ratios H/C, O/C, N/C and S/C are limited to 0.3-3, 0-3, 0-0.5 and 0-0.2, respectively. Mass error must be smaller than 0.5 ppm. Formula containing C, H, O, N, S and I isotopologues were removed from the formula lists. A formula with m/z > 500

was not reported if it did not belong to any CH_2 homologous series. For a formula $C_cH_hO_oN_nS_sI_x$, double bond equivalents (DBE) defined as $DBE = \frac{2c+2-h+n-x}{2}$ was required to be non-negative. Formula calculation was done following the same procedure for the three field blank samples. All formulas found in the field blank samples, regardless of peak intensity, were excluded from the formula lists of real samples. Aromaticity index (AI) is calculated from $AI = \frac{DBE_{AI}}{C_{AI}} = \frac{1+c-o-s-0.5h}{c-o-s-n}$. If $DBE_{AI} \leqslant 0$ or $C_{AI} \leqslant 0$, then AI = 0. A threshold value of $AI \geqslant 0.5$ provides an unambiguous minimum criterion for the presence of aromatic structure in a molecule(Yassine et al., 2014).

3. RESULTS AND DISCUSSION

3.1. Organic compounds dominate the growth of new particles initiated by iodine nucleation

Although our offline technique did not allow us to probe nucleating cluster composition at ~1.7 nm, four facts from our observation support that the NPF events from May 9 to 11 were initiated by iodine nucleation. First, strong I-NPF events were observed almost every sunny day in April and May, which was the growth and farming season of seaweed. HYSPLIT Back-trajectories analysis (Draxler and Rolph, 2010) shows that air masses moved from East China Sea to the sampling site during the I-NPF days from May 8 to 10, 2018 (Figure S1b). Sea breeze was also expected to flow from the sea to the site in the daytime when the I-NPF events occurred. Second, the evolution of PNSD from May 9 to 11 was not like banana-shape C-NPF observed on the winter days, but was markedly similar to prior reports of iodine-nucleation at European coastal sites (M äkel äet al., 2002; Sipil äet al., 2016). Third, the production of 2-7 nm particles ($N_{2\text{-}7}$) during the C-NPFs followed a nearly identical variation with solar radiation (Figure S2c), which is an indication that the C-NPFs was initiated by OH and H_2SO_4 production dictated by solar radiation. However, this was not observed

during the I-NPF events, instead, $N_{2\text{-}7}$ was anti-correlated to tidal height in the daytime (Figure S2a). Fourth, probably the most important, mean total I in 10-56 nm particles during the I-NPF days (13.5 ng m^{-3}, Table 1) was 67 and 36 times higher than those during the C-NPF days (0.2 ng m^{-3}) and non-event days (0.37 ng m^{-3}). In the same size range, mean HSO_4^- concentration (0.2 μg m^{-3}) during the I-NPF days was lower than that during the C-NPF days (0.5 μg m^{-3}).

By assuming nanometer-sized particles are spherical with a density of 1.5 g cm^{-3}, we estimate from the PNSD data that aerosol mass in the 10-56 nm size range was enhanced by 3.0 and 1.3 μg m^{-3} at most by the selected I-NPF and C-NPF events (Figure S2b and S2d). The fraction of organic mass (OM) in the aerosol mass can be further calculated as $(1.5 \times m_{TOC})/(m_{Total\ I} + m_{HSO4^-} + 1.5 \times m_{TOC}) \times 100\%$ by assuming an OM/TOC ratio of 1.5. The result shows that mass fractions of OM are 95%, 87% and 68%, respectively, in the size bins 10-18 nm, 18-32 nm and 32-56 nm during the I-NPF days. Therefore, organic compounds dominate the aerosol mass in the 10-56 nm new particles during the I-NPF days and were critical for I-NPF to contribute to CCN. Our result is qualitatively consistent with previous measurements showing that nucleation mode particles initiated by iodine were composed of a remarkable fraction of organic compounds and sulfate (Mäkelä et al., 2002; Vaattovaara et al., 2006). The main purpose of this article is to identify these organic compounds during the I-NPF days. The OC composition during the C-NPF days is beyond the scope of this article.

Table 1. Concentrations of Total iodine (I), HSO_4^- and Total Organic Carbon (TOC) in 3 size bins between 10-56 nm during the I-NPF, C-NPF and non-NPF days. For simplicity, only the sum of three size bins are shown for the C-NPF and non-NPF days. BDL=below detection limit.

	I-NPF			C-NPF	non-NPF
	10-18 nm	18-32 nm	32-56 nm	10-56 nm	10-56 nm
Total I (μg m^{-3})	2.3×10^{-3}	6.2×10^{-3}	5.0×10^{-3}	0.20×10^{-3}	0.37×10^{-3}
HSO_4^- (μg m^{-3})	2.2×10^{-2}	3.4×10^{-2}	14.4×10^{-2}	50×10^{-2}	BDL
TOC (μg m^{-3})	3.1×10^{-1}	1.8×10^{-1}	2.1×10^{-1}	2.8×10^{-1}	BDL

3.2. Elemental composition of non-iodinated OC on the I-NPF days

Non-target analysis of OC elemental composition was performed in detail on 10-18 nm, 32-56 nm, 180-560 nm and 3.2-5.6 μm particles during the I-NPF days. Elemental formulas in the 4 size bins can represent OC molecular composition of nucleation mode, Aitken mode, accumulation mode and coarse mode, respectively. OC formulas were divided into two categories: non-iodinated OC and iodinated OC. There are far more non-iodinated OC formulas than iodinated OC formulas in <1 μm particles in terms of both formula number (Table 2) and relative intensity (Figure 1). For example, 2831 non-iodinated OC formulas account for 96.6% of OC total intensity in 10-18 nm particles, while 137 iodinated OC formulas account for the remaining 3.4%. It means that non-iodinated OC dominates new particle growth during the I-NPF events. In this section, we first discuss chemical characteristics of non-iodinated OC, while the speciation of iodinated OC will be discussed in Section 3.4.

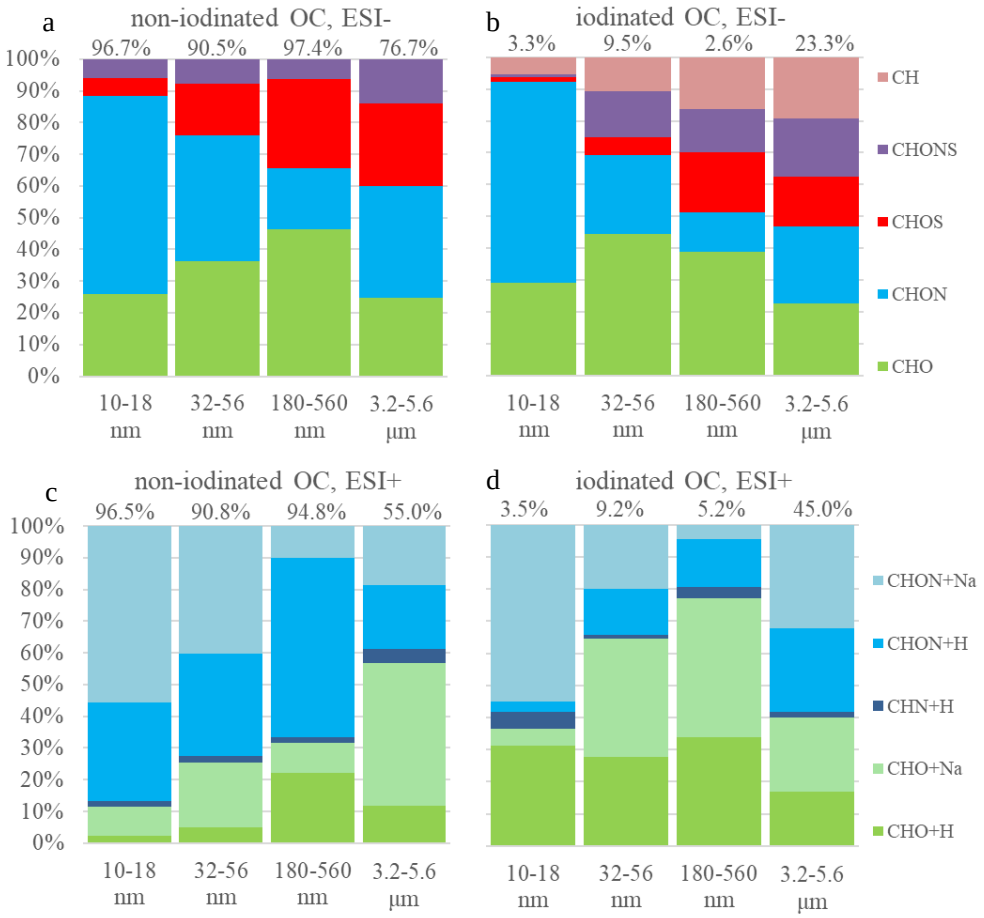

Figure 1. Relative intensity distributions of elemental groups observed in 10-18 nm, 32-56 nm, 180-560 nm and 3.2-5.6 μm size bins in ESI+ and ESI- modes. The percentage above a column denote the percent of non-iodinated OC (or iodinated OC) intensity in total OC intensity in a size bin. +Na and +H denote $[M+Na]^+$ and $[M+H]^+$ adduct in ESI+ mode, respectively.

The molecular formulas of non-iodinated OC were divided into seven elemental groups CHO^-, CHO^+, $CHON^-$, $CHON^+$, $CHOS^-$, $CHONS^-$ and CHN^+. The number distribution of 7 elemental groups for the 4 size bins is listed in Table 2. If both $[M+Na]^+$ and $[M+H]^+$ adducts of a formula were detected, the formula was counted only once. It should be noted that some formulas were repeatedly detected in ESI+ and ESI- modes. Some formulas detected in one size bin were also detected in another size bin. This is quantitatively shown in the first four rows of Table 2. For instance, 58%, 25% and 4% of the formulas detected in 10-18 nm aerosols were also detected in 32-56 nm, 180-560 nm and 3.2-5.6 μm aerosols, respectively. In another word, the particles in neighboring size bins share more similarity in organic composition. An unexpected finding is that the number of non-iodinated OC formulas detected in 3.2-5.6 μm coarse particles (n = 266) is one order of magnitude lower than those of other bins. Reconstructed mass spectra of the 7 elemental groups in ESI-and ESI+ modes are shown in Figure S3 for the four size bins.

Table 2. The numbers of assigned formulas of elemental groups of organic compounds in 10-18 nm, 32-56 nm, 180-560 nm and 3.2-5.6 μm size bins. The first 4 rows show the percent of formula repeatability between two size bins. 1I-OC: molecular formula containing one iodine atom.

Repeatability	10-18 nm	32-56 nm	180-560 nm	3.2-5.6 μm	
10-18 nm		58%	25%	4%	
32-56 nm	57%		38%	4%	
180-560 nm	34%	51%		6%	
3.2-5.6 μm	35%	35%	34%		
Non-iodinated OC					Total
CHO^-	531	565	525	20	892
CHO^+	250	501	380	111	857

$CHON^-$	1005	638	347	25	1268	
$CHON^+$	1139	1055	828	72	2121	
$CHOS^-$	147	216	256	22	357	
$CHONS^-$	134	131	93	10	259	
CHN^+	34	26	7	7	46	
Total	2831	2770	2151	266	4979	
Iodinated OC					Total	1I-OC (%)
$CHOI^-$	32	53	11	5	80	64%
$CHOI^+$	17	85	31	31	136	93%
$CHONI^-$	52	29	7	7	77	88%
$CHONI^+$	34	57	18	52	132	81%
$CHOSI^-$	3	8	7	3	18	72%
$CHONSI^-$	2	7	3	2	13	62%
$CHNI^+$	6	4	4	3	16	56%
CHI^-	4	2	1	4	9	67%
Total	137	228	76	100	440	80%

CHON is the most commonly assigned elemental group in both ESI+ (2121 $CHON^+$) and ESI- (1268 $CHON^-$) modes, followed by the CHO group (857 CHO^+ formulas and 892 CHO^- formulas). S-containing formulas are 357 $CHOS^-$ and 259 $CHONS^-$. The formula number of the least common CHN^+ group is only 46. In terms of relative intensity, CHON fraction in the ESI- mode decreases from 61% of OC in the 10-18 nm bin to 20% in the 180-560 nm bin (Figure 1a), while the fractions of CHO and CHOS/CHONS increase with particle size. In the ESI+ mode, the fraction of CHON decreases from 88% in 10-18 nm bin to 70% in 180-560 nm bin, being always the dominant elemental group of non-iodinated OC (Figure 1b). Low molecular weight (LMW) amines are important stabilizers in acid-base nucleation (Kurtén et al., 2008; Jen et al., 2014; Zheng et al., 2000; Yao et al., 2016), but their molecular ions are out of the mass range of our FT-ICR-MS. The CHN^+ formulas that we observed contained 9-50 C atoms and 1-7 N atoms, accounting for a negligible fraction 1.7% of total intensity of all ESI+ formulas in the 10-18 nm particles.

Previous elemental composition studies using FT-ICR-MS were mostly conducted on $PM_{2.5}$ or PM_{10} collected from marine (Schmitt-Kopplin et al., 2012; Bao et al., 2018; Ning et al., 2019), urban (Wu et al., 2019; Jiang et al., 2016), free troposphere (Schum et al., 2018; Mazzoleni et al., 2012) and forest sites (Kourtchev et al., 2013). In general, these studies showed that the numbers of CHO compounds were comparable with or

more than those of CHON compounds. Our study shows clearly that elemental composition of aerosol OC is highly size dependent. New particle growth in the size range of 10-18 nm during the I-NPF event is dominated by CHON elemental group, followed by CHO. The focus of this article narrows on the identity and source of the CHON and CHO formulas in 10-18 nm particles, by comparing with those in the 180-560 nm size bin.

3.2.1. CHO formulas

There is a total of 531 CHO^- formulas and 250 CHO^+ formulas in 10-18 nm particles. 54 CHO formulas are commonly found in ESI+ and ESI- modes. In terms of relative intensity, CHO^- compounds are more abundant than CHO^+ compounds (Figure 3b, total intensity: 4.14 e+09 *vs.* 1.24 e+09). However, this is not indicative of absolute concentration of the two groups due to different ionization efficiency between ESI- and ESI+ modes. CHO^- is characterized by a series of formulas with 20, 24, 28, and 33 C atoms, 4 or 6 O atoms and 1 equivalent double bond (Figure 2b). The total intensity of top 10 formulas accounts for 30% of all 531 formulas. Assuming CHO^- formulas contain at least 1 carboxylic group (–COOH), the rest of their molecules should be saturated (DBE = 0) and contain 2 or 4 O atoms.

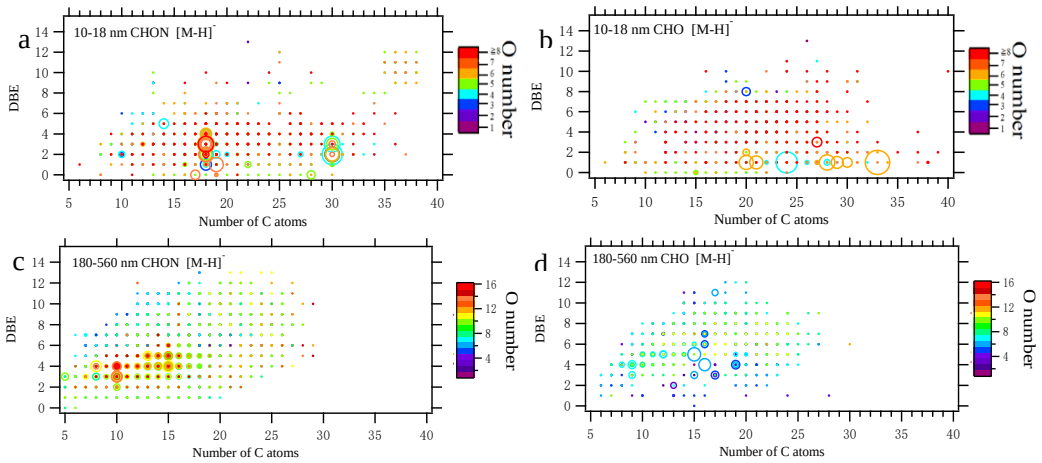

Figure 2. DBE *vs.* C atom number diagrams of all CHON and CHO formulas detected in 10-18 nm and 180-560 nm particles in ESI- mode. The color bar denotes O atom

number in the formulas. The size of the circles reflects the relative intensities of molecular formulas on a logarithmic scale.

The above feature is not seen in either CHO^+ formulas in the 10-18 nm bin or CHO^- formulas in the 180-560 nm bin. There are more C_{21} and C_{24} formulas than other C subgroups in the CHO^+ formulas of 10-18 nm bin (Figure S4d), but none of them have exceptionally-high intensity. The prominent formulas in the CHO^- group in 180-560 nm particles have a relatively high unsaturation degree (DBE = 3-7, Figure 2d). The relative intensities of subgroups according to C atom number in the CHO^- formulas in the 180-560 nm bin are characterized by trimodal distribution with maximum intensity around C_9, C_{13}-C_{16} and C_{20} (Figure 3d). The relative intensity of O atom subgroups is mono-modally distributed around O_7 (Figure S5).

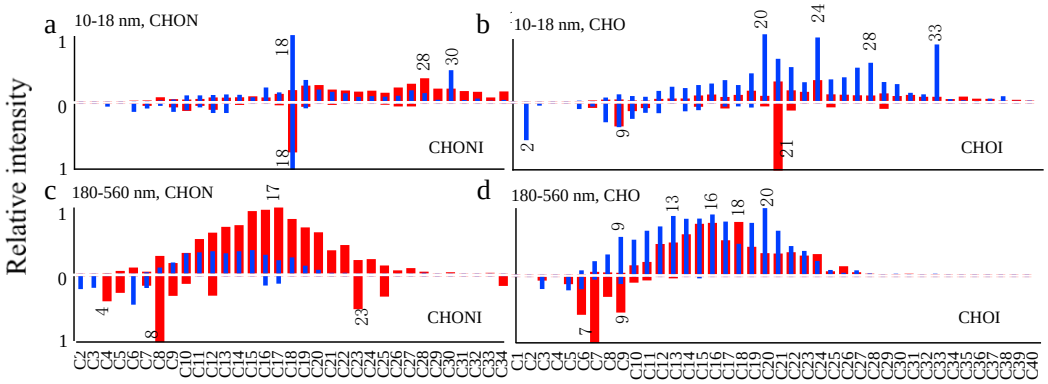

Figure 3. Relative intensities of subgroups according to C atom number in CHON, CHO, CHONI and CHOI formulas in 10-18 nm and 180-560 nm particles in ESI+ (in red) and ESI- (in blue). The intensity of the most abundant subgroup in a size bin is defined as 1 and those of other subgroups are normalized by it. The relative intensities of non-iodinated OC formulas (iodinated OC formulas) are plotted in the region above (below) zero line.

3.2.2. CHON formulas

As discussed earlier, CHON is the most abundant elemental group observed in the smallest size bin 10-18 nm. There is a total of 1005 $CHON^-$ formulas (total intensity

9.96 e+09) and 1139 $CHON^+$ formulas (6.45 e+09) in 10-18 nm bin. 355 CHON formulas are commonly found in ESI+ and ESI- modes. A close examination of Figure 2a and 3a reveals that $CHON^-$ is characterized by a series of C_{18} and C_{30} formulas with low DBE values (1-4). 87 C_{18} and 26 C_{30} formulas account for 37% of total intensity of $CHON^-$. Such feature is not seen for $CHON^+$ formulas that are rather uniformly distributed in DBE vs. C diagram (Figure S4a and S4c). Generally speaking, $CHON^-$ compounds should contain nitro- ($–NO_2$) or nitrooxy- ($–ONO_2$) group and are ionizable due to the presence of –COOH or hydroxy (–OH) (Lin et al., 2012). However, the presence of amine group in $CHON^-$ formulas cannot be excluded. Take C_{18} as example, 51 out of 87 $C_{18}H_hO_oN_n^-$ formulas should contain at least one amine group, either because their O atom numbers are not large enough to allow the assignment of $–NO_2$ for all N atoms, or because some formulas (25 out of 87) were also detected in ESI+ mode. In total, 51 $C_{18}H_hO_oN_n^-$ formulas with an amine group account for 54.4% of total intensity of 87 $C_{18}H_hO_oN_n^-$ formulas.

The presence of amine group in $C_{18}H_hO_oN_n^-$ formulas in 10-18 nm particles is also supported by the comparison with $CHON^-$ in 180-560 nm submicron aerosols. $CHON^-$ in 180-560 nm is characterized by a number of formulas with maximum intensity around C_{10} and C_{15} (Figure 2c). A plot of O atom number *vs.* N atom number in Figure S6a shows that $C_{10}H_hO_oN_n^-$ in 180-560 nm have O/N ratios ≥ 3 and O atom number is positively correlated with N atom number. It indicates that these $C_{10}H_hO_oN_n^-$ formulas are probably nitro- or nitrooxy- oxidation products of monoterpenes from continental plant emission. In contrast, O/N ratios of the $C_{18}H_hO_oN_n^-$ formulas in 10-18 nm are mostly small and O atom number do not increase with N atom number (Figure S6b). All collective evidences above reveal that nitrogen-containing organic compounds in 10-18 nm particles during the I-NPF days are partly composed of long-chain amino alcohols, amino acids and so on.

In summary, a series of very distinctive $CHON^-$ and CHO^- formulas was observed in 10-18 nm new particles during the I-NPF days. These formulas are characterized by some specific numbers of C atoms (i.e. $C_{18}H_hO_oN_n$, $C_{30}H_hO_oN_n$, $C_{20}H_hO_o$, $C_{24}H_hO_o$, $C_{28}H_hO_o$ and $C_{33}H_hO_o$) and equivalent double bonds (DBE = 1 for CHO^- and 1-4 for

CHON$^-$). Monomer-dimer distribution pattern that can arise from particle-phase oligomerisation (Pospisilova et al., 2020) was not observed for these formulas in the mass spectra. We also assume that $C_{18,30}H_hO_oN_n$ and $C_{20,24,28,33}H_hO_o$ are not labile intermediates like ester hydroperoxides that may undergo fast decomposition in the particles or during the sample preparation process (Zhao et al. 2018 a,b). To the best of our knowledge, such CHON$^-$ and CHO$^-$ formulas have not been reported by previous aerosol studies. The chemical composition of new particles is completely decoupled with the CHO$^-$ and CHON$^-$ formulas around C_{10}, C_{15} and C_{20} in 180-560 nm submicron particles, which might be originated from continental terpene emissions. Fewer O atoms in $C_{18,30}H_hO_oN_n$ and $C_{20,24,28,33}H_hO_o$ formulas than those in submicron aerosols indicate that these compounds should be more freshly emitted into the atmosphere. The discontinuous chemical composition and PNSD spectrum (Figure S2b) below and above 50 nm particle size reflect the fact that the further growth of new particles beyond 50 nm in local I-NPF events cannot be monitored by our stationary sampling strategy.

On the other hand, we observed more complicated distributions of CHO$^+$ and CHON$^+$ formulas in 10-18 nm new particles that are of relatively small individual intensity and are rather uniformly distributed in DBE vs. C diagrams. Like CHON$^-$ and CHO$^-$, those CHO$^+$ and CHON$^+$ formulas also possess a larger number of C atoms (C > 19) than their counterparts in 180-560 nm submicron aerosols (Figure 3). 21 out of 30 most abundant CHON$^+$ formulas contain two or more N atoms; this ratio 21/30 is higher than those in CHON$^-$ formulas. Generally speaking, CHO$^+$ and CHON$^+$ formulas represent carbonyls/alcohols/epoxides and amino alcohols/amino acids, respectively. One interesting finding about CHO$^+$ and CHON$^+$ is that they tend to form $[M+Na]^+$ adducts in small aerosols and $[M+H]^+$ adducts in large aerosols (Figure 1c). This indicates that the CHO$^+$ and CHON$^+$ compounds in new particles during the I-NPF days should possess different basic functional groups from those in submicron particles.

3.3. Possible precursors and formation mechanism of organic compounds detected in 10-18 nm new particles during the I-NPF days

It is unrealistic to simply propose one out of a large number of possible structures for a formula with large C atom number (e.g., ≥ 18). Our strategy is to first explore the possible precursors of the newly found $C_{18,30}H_hO_oN_n$ and $C_{20,24,28,33}H_hO_o$ formulas. Obviously, $C_{18,30}H_hO_oN_n$ and $C_{20,24,28,33}H_hO_o$ formulas cannot be attributed to continental terpene emission or anthropogenic aromatic emissions. Sporadic spikes of 10-18 nm particles that can be an indication of cooking and traffic emissions were not seen in the PNSD spectrum, because such human activities were rare around the site during the sampling period. We thus also exclude the possibility of cooking and traffic emissions.

Previous field measurements of marine NPF precursor focused on volatile species like iodine (Stevanović et al., 2019), iodomethanes (O'Dowd et al., 2002), dimethyl sulfonic acid (Yvon et al., 1996; Barone et al., 1996; Barnes et al., 2006) and LMW amines (Ning et al., 2019; Ge et al., 2011). So far there is no report about aliphatic compounds with C number ≥ 18 in either gas phase or new particles (Cochran et al., 2017; Bikkina et al., 2019). Therefore, we consulted the literature that reported chemical compounds isolated from biological tissues of algae, plankton or other marine organisms. Potential precursors are listed in Table 3.

3.3.1. Fatty acids

Fatty acids (FAs) are widely found in animals, plants and microbe (Moss et al., 1995). Plants have higher content of unsaturated FAs than animals. C_{14}-C_{24} fatty acids, including both saturated and unsaturated, have long been observed in seaweed (Dawczynski et al., 2007). Very long chain FAs (C_{24}-C_{36}) have been isolated from green algae, chlorella kessleri, sponges and marine dinoflagellate (Litchfield et al., 1976; Řezanka and Podojil, 1984; Mansour et al., 1999). C_{18} Oleic acid, linoleic acid and linolenic acid are most commonly found unsaturated FAs in macro algae. FAs with carbon chain shorter than C_{20} were used by atmospheric chemists as organic

tracers of atmospheric aerosols from microbe or kitchen emission (Simoneit and Mazurek, 1982; Zheng et al., 2000; Guo et al., 2003; Rogge et al., 1991; DeMott et al., 2018; Willoughby et al., 2016). In our study, no saturated FAs were detected in 10-18 nm particles. Only 1.5% of CHO^- formulas can be assigned to unsaturated FAs (that is, include 2 O atoms, 14-28 C atoms and DBE = 3-6). Other CHO compounds observed in 10-18 nm particles contain > 2 O atoms and thus can be assigned as the oxidized derivatives of FAs.

Table 3 Possible precursors and their presence in marine biological sources and our aerosol samples. ND: not detected.

	Potential precursors	Presence in marine sources	Presence in aerosol particles
Unsaturated fatty acid	C_{14}-C_{24} fatty acids	Seaweed (Dawczynski et al., 2007)	1.5% of CHO^- in terms of relative intensity
	C_{25}--C_{36} very long chain fatty acids	Green algae, chlorella kessleri, sponges, marine dinoflagellate (Litchfield et al., 1976; Řezanka and Podojil, 1984; Mansour et al., 1999).	ND
fatty alcohols	C_{30}-C_{32} mono- and diunsaturated alcohols and diols	Yellow-green algae (Volkman et al., 1992)(eustigmatophytes)	ND
Saturated hydroxyl fatty acids	$C_{20}H_{40}O_3$, $C_{32}H_{64}O_4$	Nannochloropsis, cutins and suberins of higher plants (Gelin et al., 1997).	S/N 15 and 28
Nonprotein amino acid	$C_{18}H_{37}NO_4$ saturated dihydroxy amino acid (simplifungin,	Marine fungal metabolites (Ishijima et al., 2016; VanMiddlesworth et al., 1992).	S/N 280
	$C_{20\text{-}22}H_{39\text{-}41}NO_{5\text{-}7}$ mono-unsaturated polyhydroxy amino acids in sphigolipids		S/N 30-230
Amino alcohols	$C_{16\text{-}28}H_{33\text{-}53}NO_{1\text{-}4}$ polyhydroxy amino alcohols	Plant biomembrane, secondary metabolites in marine organisms (Jares-Erijman et al., 1993).	S/N 23-640
	$C_{18}H_{31}NO$ and $C_{18}H_{29}NO$ polyunsaturated amino alcohols	Mediterranean tunicate (Jares-Erijman et al., 1993)	S/N 10-60
	$C_{18}H_{36}N_2O_5$ polyhydroxy cyclic alkaloid	Moraceae (Tsukamoto et al., 2001)	S/N 800

Possible oxidation schemes of two typical C_{18} ($C_{18}H_{30}O_2$, α-linolenic acid, three C=C double bonds in carbon chain) and C_{28} unsaturated FAs ($C_{28}H_{52}O_2$, two C=C double bonds), for instance, are proposed in Figure S7 and S8. The reaction of an unsaturated FA after the emission into the atmosphere is initiated by OH addition to C=C double bond and subsequent O_2 addition to form a peroxy radical (Atkinson et

al., 1995; Calvert et al., 2000). Depending on the level of NO and reactivity, four competitive pathways are available for peroxy radicals to produce CHO or CHON formulas observed in our study: reaction with NO to form a $–ONO_2$ group (pathway 1) or an alkoxy radical that further reacts with O_2 to form a carbonyl (–C=O, pathway 2), reaction with RO_2 radicals to form a hydroxyl (–OH) or a –C=O group (pathway 3) and successive intermolecular H-shift/O_2 addition autoxidation(Crounse et al., 2013; Vereecken et al., 2015) (pathway 4).

Pathways 1 and 2 add $–ONO_2$, –OH and –C=O groups to carbon chain but do not reduce the DBE of FA precursor. We propose that pathway 1 and 2 are preferred for those FAs with higher reactivity with NO (e.g., α-linolenic acid, Figure S7). α-linolenic acid oxidation in the atmosphere via sequential occurrences of pathways 1 or 2 yields a series of oxygenated and nitrated organic compounds, among which $C_{18}H_{31}NO_6$, $C_{18}H_{31}NO_8$, $C_{18}H_{31}NO_{10}$, $C_{18}H_{32}N_2O_{10}$ and $C_{18}H_{33}N_3O_4$ are found in 10-18 nm particles. These formulas explain the circles with DBE = 4 and C number = 18 shown in Figure 2a (DBE *vs.* C atom number diagram).

The net outcome of sequential pathway 3 and 4 reactions is to add –OH and –C=O groups and reduce the DBE of FA precursor. We propose that pathway 3 and 4 are preferred for those FAs (e.g. C_{28} FA $C_{28}H_{52}O_2$) with higher reactivity with RO_2 (Figure S8). The end products are a series of $C_{28}H_{52}O_{6\text{-}8}$, $C_{28}H_{54}O_{4\text{-}7}$ and $C_{28}H_{56}O_{6\text{-}8}$ compounds, which can explain the circles with C number = 28 and DBE = 1-3 in Figure 2b.

In addition to fatty acids, fatty alcohols such as C_{30}-C_{32} mono- and di-unsaturated alcohols and diols have been detected in yellow-green algae (Volkman et al., 1992). Although these unsaturated alcohols were not detected in our 10-18 nm particles, we suppose that they or their metabolites in algae may undergo similar reactions like unsaturated FA to generate condensable oxygenated and nitrated fatty alcohols in the atmosphere. Hydroxy fatty acids (HFAs) are important constituents of lipid in marine microalgae (Gelin et al., 1997), bacteria (Kim and Oh, 2013), seaweed (Kendel et al., 2013; Blokker et al., 1998) and leaf surface of higher plants (Pollard et al., 2008). Among them, two saturated HFAs $C_{20}H_{40}O_3$ and $C_{32}H_{64}O_4$ were found

in our 10-18 nm aerosol sample with S/N ratios 15 and 28. However, because saturated hydroxy fatty acids are not oxidizable via the pathways proposed in our study, they are assumed unlikely to be precursors of other formulas observed in 10-18 nm particles.

3.3.2. Nonprotein amino acids and amino alcohols

Quantum chemical calculations have showed that amino acids like Glycine, Serine, and Threonine are potential participants in atmospheric nucleation via interaction with sulfuric acid (Elm et al., 2013; Ge et al., 2018; Li et al., 2020). However, we did not observe any of 20 essential amino acids in 10-18 nm in either ESI+ or ESI- modes. One reason may be that most of essential amino acids have molecular weight less than 150 that is below mass scan range of our FT-ICR-MS.

There are a number of records in the literature about long chain non-protein amino acids or amino alcohols isolated from marine organisms or plant biomembrane (Ishijima et al., 2016; VanMiddlesworth et al., 1992; Jares-Erijman et al., 1993; Tsukamoto et al., 2001). They include saturated dihydroxy amino acid ($C_{18}H_{37}NO_4$, DBE = 1, simplifungin), monounsaturated polyhydroxy amino acids in sphigolipids ($C_{20\text{-}22}H_{39\text{-}41}NO_{5\text{-}7}$, DBE = 2-3), polyhydroxy amino alcohols ($C_{16\text{-}28}H_{33\text{-}53}N_{1\text{-}2}O_{1\text{-}5}$, DBE = 1-3, sphingosine and its natural metabolites) and polyunsaturated amino alcohols ($C_{18}H_{31}NO$ and $C_{18}H_{29}NO$, DBE = 4-5). All of these formulas were detected in 10-18 nm aerosols with S/N in the range of 10-800. More importantly, all those compounds that contain at least one amine group and one C=C double bond can be precursors of observed CHON formulas containing amine group via the pathways that we showed above. As an example, the oxidation scheme of an amino alcohol $C_{18}H_{31}NO$ with 4 C=C double bonds in carbon chain is illustrated in Figure S9.

Similar to C_{28} FA, $C_{18}H_{31}NO$ undergoes successive intermolecular H-shift/O_2 additions to produce a series of RO_2 radicals with hydroperoxyl group (–OOH) in its carbon chain. The subsequent pathway 3 reactions, as well as the decomposition of –OOH groups, add –OH and –C=O groups in the carbon chain. Because $C_{18}H_{31}NO$ possesses as many as 4 C=C double bonds, sequential pathway 3 and 4 reactions produce a large number of oxidation products, among which 57 are found in the

formula list detected in 10-18 nm particles (Figure S9). These products $C_{18}H_{31}NO_{4\text{-}11,13}$, $C_{18}H_{33}NO_{4,6\text{-}10}$, $C_{18}H_{35}NO_{5\text{-}9}$, $C_{18}H_{37}NO_{7\text{-}12}$ and $C_{18}H_{39}NO_{10\text{-}11}$ explain perfectly the presence of a series of formulas with C number = 18, DBE = 0-4 and a $–NH_2$ group shown in Figure 2a.

3.3.3. Volatility estimation

Based on the reaction mechanisms proposed above, it is possible to estimate the volatility change from potential precursors to their oxidation products. First, from the list of elemental formulas detected in 10-18 nm particles, we select 49 formulas with high intensities, including 14 $CHON^-$ formulas with peak intensity > 1.00 e+08, 23 $CHON^+$ formulas with peak intensity > 3.00 e+07 and 12 CHO^- formulas (DBE = 1) with peak intensities > 3.00 e+07. Possible combinations of –COOH, $–ONO_2$, –C=O, C=C double bond, $–NH_2$ and –OH groups are searched for every formula obeying two simple rules: $CHON^-$ and CHO^- formulas must possess a carboxyl or hydroxyl group; $CHON^+$ formulas must possess an amino group. Saturation concentrations (C*) of the 49 formulas were then predicted for all combinations using a simple group contribution method developed by Pankow and Asher (Pankow and Asher, 2008). On the other hand, the C*of their possible precursors, including unsaturated FAs, fatty alcohols, nonprotein amino acids or amino alcohols, were predicted by the same method.

As we can see in Table S4, C* of the 49 formulas fall into the range of ELVOC (3×10^{-9} - 3×10^{-5} μg m^{-3}) and even ULVOC (ultra-low volatility organic compound, $<3 \times 10^{-9}$ μg m^{-3}), while C* of their precursors are in the range of SVOC (0.3-300 μg m^{-3}) or LVOC (3×10^{-5}-0.3 μg m^{-3}). The addition of functional groups reduces the volatility of precursors by 2~7 orders of magnitude and thus make their oxidation products condensable onto new particles during the I-NPF event days. According to the definition of Schervish and Donahue, 2019 and Simon et al., 2020, ULVOC can even drive pure biogenic nucleation. Therefore, the analysis of precursor-product volatility partly supports our hypothesis about the molecular identity and formation mechanism of the formulas detected in 10-18 nm particles. It should be noted that the volatility of VOC oxidation products can be assessed with numerous existing parameterizations,

which require either exact functional groups or only the molecular formula (Perä kyl ä et al., 2019). Their estimation can vary by up to several orders of magnitude. But this will not change the conclusion drawn here.

3.4. Speciation of iodinated OC

Organic iodine compounds hold the key to understand aerosol iodine chemistry and its role in regulating the recycling of halogens to the gas phase. We identified 440 iodinated OC formulas from the 4 size bins during the I-NPF days (Table 2). 80% of the 440 formulas contain one I atom and the rest of them contain two I atoms. In terms of relative intensity, iodinated OC accounts for 2.6-9.5% of OC in fine particles, but its fraction in coarse particles increases to 23.3% in ESI- mode and 45% in ESI+ mode. The size distribution of 7 iodinated OC groups (i.e., $CHOI^-$, $CHONI^-$, $CHOSI^-$, $CHONSI^-$, $CHOI^+$, $CHONI^+$ and $CHNI^+$) resembles those of non-iodinated OC groups (Figure 1). If we replace I atom(s) with H atom(s) in a formula, 107 out of 440 replaced formulas are also found in the non-iodine OC formula list.

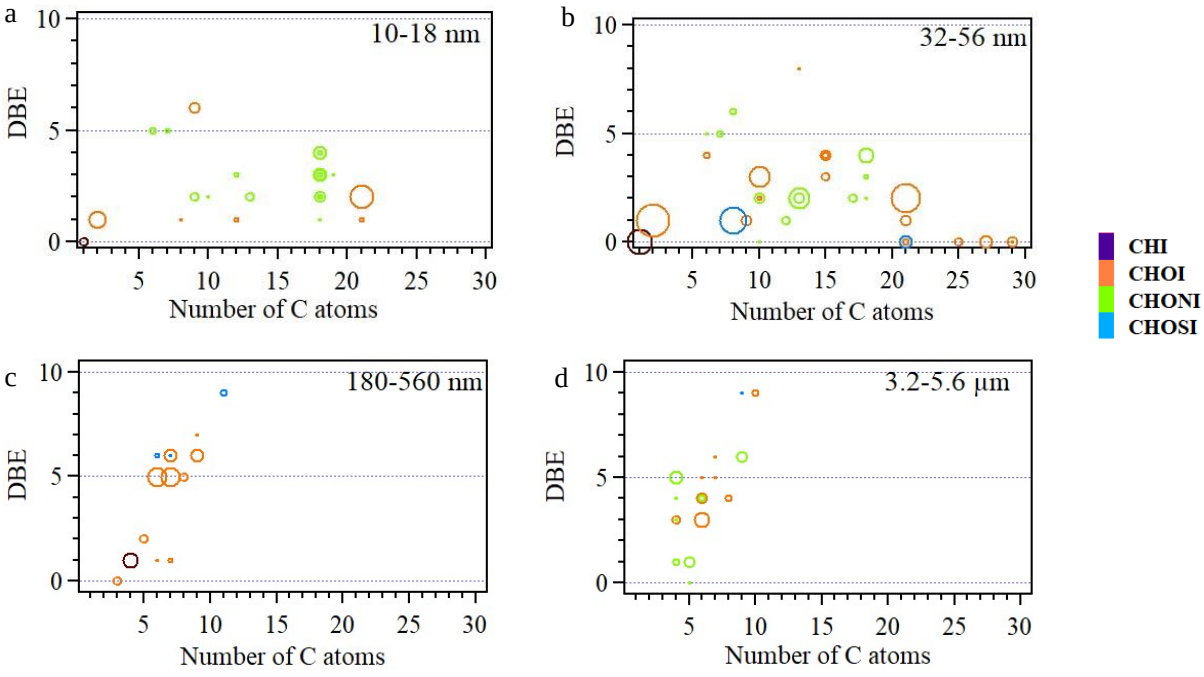

Figure 4. DBE vs. C atom number diagrams of iodinated OC formulas with intensity > 1.00 e+07 in the four size bins. The color bar denotes the elemental groups of assigned

formulas. The size of the circles reflects the relative intensities of molecular formulas on a logarithmic scale.

Iodinated OC with intensity > 1.00 e+07 in the four size bins were shown in Figure 4. The DBE vs. C diagram for 10-18 nm particles is characterized by (1) nine $C_{18}H_hO_oN_nI$ formulas with DBE = 1-4 and (2) $C_9H_{16}NO_3I$ and its C_{10}-C_{13} homologues. Because these formulas were detected in ESI+ mode, they are most likely iodinated amino acids. 32-56 nm particles accommodate most abundant iodinated OC formulas, in terms of both formula number and relative intensity. Prominent formulas include (1) diiodo acetic acid $C_2H_2O_2I_2$, diiodomethane CH_2I_2, (2) iodinated C_{21} carbonyls $C_{21}H_{39}OI$ and $C_{21}H_{41}OI$, (3) iodinated $C_{21,25,27,29}$ alcohols or ethers with DBE = 0, (4) iodinated C_{10} and C_{15} terpene and sesquiterpene oxidation products and (5) iodinated organic sulfate $C_8H_{17}N_2SO_8I$ and $C_{21}H_{43}SO_4I$. In addition, $C_9H_{10}NO_3I$ detected in this size bin (S/N ratio: 35) can be tentatively assigned to an iodinated amino acid iodotyrosine that has been observed in seaweed (Yang et al., 2016), implying direct contribution from seaweed emission to new particles.

In 180-560 nm particles, the majority of iodinated OC are $C_{6\text{-}9}$ aromatic $CHOI^+$ compounds with AI > 0.5 and DBE = 5-7. Both C and O atom numbers of these iodinated OC are smaller than those of mono-modally distributed CHO^+ compounds around C_{15} in the same particle size (Figure 3d and S3b). This implies that iodine has a strong tendency to aromatic compounds in submicron aerosols due to electrophilic substitution on aromatic rings. In 3.2-5.6 μm particles, iodinated OC features C_4-C_6 CHO^+ and $CHON^+$ compounds with DBE = 3-6, which again have fewer C atoms than non-iodinated OC. Supporting evidence from AI shows these compounds are not aromatic. Coastal 3.2-5.6 μm particles can be sea salt particles formed during bubble bursting of sea water (Russell et al., 2010; Schmitt-Kopplin et al., 2012; Quinn et al., 2014; Wilson et al., 2015). However, Hao et al. 2017 (Hao et al., 2017) showed that iodinated OC products from the reaction between iodine and seawater are highly unsaturated carboxylic-rich polyphenols with DBE = 4-14 and C atoms = 10-30. It is

thus apparent that iodinated OC in 3.2-5.6 μm particles were not directly from iodinated organic compounds in the seawater.

3.5 Atmospheric implications

Due to the 71% ocean coverage of the earth's surface, marine aerosol generation is important in determining the earth's radiative budget and climate change. Of the limited number of studies reporting coastal NPF, most have focused on iodine emission, oxidation and nucleation in the early stage of NPF. In principle, abundant low-volatility condensing vapors other than iodine are required in coastal environments for the growth of iodine clusters to CCN. This article reveals a new group of important organic compounds involved in this process. It is most likely that their precursors are emitted mutually with iodine from either direct exposure of coastal biota to the atmosphere or biological-active sea surface. If this is true, we suggest the results in our location can be extrapolated to other iodine-rich coastal locations, as long as iodine-NPF can be observed. More fundamental field, laboratory and modeling studies are needed to determine (1) exact emission sources and source rates of these organic precursors, (2) their gas phase intermediates and oxidation mechanisms in the atmosphere and (3) their quantitative contribution to global and regional CCN numbers.

ACKNOWLEDGMENTS

The work was supported by the National Science Foundation of China (grant numbers 41975831 and 41675124) and the National Key Research and Development Program of China (grant number 2016YFC0203100).

Data availability. All of the datasets related to the chemical formulas detected in this work can be accessed in "Global Change Research Data Publishing and Repository" via doi:10.3974/geodb.2020.03.26.V1. Any other data used in this

publication are available from the corresponding author Huan Yu (yuhuan@cug.edu.cn) upon request.

Author contributions. Huan Yu designed and conducted chemical analysis. Yibei Wan and Huan Yu did data analysis and wrote the paper. Xiangpeng Huang conducted the field sampling. Bin Jiang and Yuhong Liao did the FT-ICR-MS analysis. Binyu Kuang, Manfei Lin, Deming Xia, Jingwen Chen and Jianzhen Yu reviewed and revised the manuscript.

Conflict of Interest

The authors declare that they have no conflict of interest.

REFERENCE

Allan, J. D., Williams, P. I., Nájera, J., Whitehead, J. D., Flynn, M. J., Taylor, J. W., Liu, D., Darbyshire, E., Carpenter, L. J., Chance, R., Andrews, S. J., Hackenberg, S. C., and McFiggans, G.: Iodine observed in new particle formation events in the Arctic atmosphere during ACCACIA, Atmos. Chem. Phys., 15, 5599-5609, doi:10.5194/acp-15-5599-2015, 2015.

An, Y. Q., Xu, J. Z., Feng, L., Zhang, X. H., Liu, Y. M., Kang, S. C., Jiang, B., and Liao, Y. H.: Molecular characterization of organic aerosol in the Himalayas: insight from ultra-high-resolution mass spectrometry, Atmos. Chem. Phys., 19, 1115-1128, doi:10.5194/acp-19-1115-2019, 2019.

Atkinson, R., Tuazon, E. C., and Aschmann, S. M.: Products of the Gas-Phase Reactions of a Series of 1-Alkenes and 1-Methylcyclohexene with the OH Radical in the Presence of NO, Environ. Sci. Technol., 29, 1674-1680, doi:10.1021/es00006a035, 1995.

Bao, H. Y., Niggemann, J., Li, L., Dittmar, T., and Kao, S.-J.: Molecular composition and origin of water-soluble organic matter in marine aerosols in the Pacific off China, Atmos. Environ., 191, 27-35, doi:10.1016/j.atmosenv.2018.07.059, 2018.

Barnes, I., Hjorth, J., and Mihalopoulos, N.: Dimethyl Sulfide and Dimethyl Sulfoxide and Their Oxidation in the Atmosphere, Chem. Rev., 106, 940-975, doi:10.1021/cr020529+, 2006.

Barone, S. B., Turnipseed, A. A., and Ravishankara, A. R.: Reaction of OH with Dimethyl Sulfide (DMS). 1. Equilibrium Constant for OH + DMS Reaction and the Kinetics of the OH ÐDMS + O2 Reaction, J. Phys. Chem. A., 100, 14694-14702, doi:10.1021/jp960866k, 1996.

Bianco, A., Deguillaume, L., Va ïilingom, M., Nicol, E., Baray, J.-L., Chaumerliac, N., and Bridoux, M.: Molecular Characterization of Cloud Water Samples Collected at the Puy de Dôme (France) by Fourier Transform Ion Cyclotron Resonance Mass Spectrometry, Environ. Sci. Technol., 52, 10275-10285, doi:10.1021/acs.est.8b01964, 2018.

Bikkina, P., Kawamura, K., Bikkina, S., Kunwar, B., Tanaka, K., and Suzuki, K.: Hydroxy Fatty Acids in Remote Marine Aerosols over the Pacific Ocean: Impact of Biological Activity and Wind Speed, ACS. Earth. Space. Chem., 3, 366-379, doi:10.1021/acsearthspacechem.8b00161, 2019.

Blokker, P., Schouten, S., van den Ende, H., De Leeuw, J. W., and Sinninghe Damsté, J. S.: Cell wall-specific ω-hydroxy fatty acids in some freshwater green microalgae, Phytochemistry., 49, 691-695, doi:10.1016/S0031-9422(98)00229-5, 1998.

Burkholder, J. B., Curtius, J., Ravishankara, A. R., and Lovejoy, E. R.: Laboratory studies of the homogeneous nucleation of iodine oxides, Atmos. Chem. Phys., 4, 19-34, doi:10.5194/acpd-3-4943-2003, 2004.

Calvert, J. G., Atkinson, R. G., Orlando, J. J., Wallington, T. J., and Tyndall, G. S.: The Mechanisms of Atmospheric Oxidation of Alkenes, Oxford Univ. Press, Oxford, UK., 2000.

Cochran, R. E., Laskina, O., Trueblood, J. V., Estillore, A. D., Morris, H. S., Jayarathne, T., Sultana, C. M., Lee, C., Lin, P., Laskin, J., Laskin, A., Dowling, J. A., Qin, Z., Cappa, C. D., Bertram, T. H., Tivanski, A. V., Stone, E. A., Prather, K. A., and Grassian, V. H.: Molecular Diversity of Sea Spray Aerosol Particles: Impact of Ocean Biology on Particle Composition and Hygroscopicity, Chem. Pharm. Bull, 2, 655-667, doi:10.1016/j.chempr.2017.03.007, 2017.

Crounse, J. D., Nielsen, L. B., Jørgensen, S., Kjaergaard, H. G., and Wennberg, P. O.: Autoxidation of Organic Compounds in the Atmosphere, J. Phys. Chem. Lett., 4, 3513-3520, doi:10.1021/jz4019207, 2013.

Daellenbach, K. R., Kourtchev, I., Vogel, A. L., Bruns, E. A., Jiang, J. H., Petäjä, T., Jaffrezo, J.-L., Aksoyoglu, S., Kalberer, M., Baltensperger, U., Haddad, I. E., and Prevot, A. S. H.: Impact of anthropogenic and biogenic sources on the seasonal variation of the molecular composition of urban organic aerosols: a field and laboratory study using ultra-high resolution mass spectrometry, Atmos. Chem. Phys. Discuss., 19, 5973-5991, doi:10.5194/acp-2018-1128, 2018.

Dall Ósto, M., Simo, R., Harrison, R. M., Beddows, D. C. S., Saiz-Lopez, A., Lange, R., Skov, H., Nøjgaard, J. K., Nielsen, I. E., and Massling, A.: Abiotic and biotic sources influencing spring new particle formation in North East Greenland, Atmos. Environ., 190, 126-134, doi:10.1016/j.atmosenv.2018.07.019, 2018.

Dawczynski, C., Schubert, R., and Jahreis, G.: Amino acids, fatty acids, and dietary fibre in edible seaweed products, Food. Chem., 103, 891-899, doi:10.1016/j.foodchem.2006.09.041, 2007.

DeMott, P. J., Mason, R. H., McCluskey, C. S., Hill, T. C. J., Perkins, R. J., Desyaterik, Y., Bertram, A. K., Trueblood, J. V., Grassian, V. H., Qiu, Y., Molinero, V., Tobo, Y., Sultana, C. M., Lee, C., and Prather, K. A.: Ice nucleation by particles containing long-chain fatty acids of relevance to freezing by sea spray aerosols, Environ. Sci-Proc. Imp., 20, 1559-1569, doi:10.1039/c8em00386f, 2018.

Draxler, R., Rolph, G.: HYSPLIT (HYbrid Single-Particle Lagrangian Integrated Trajectory) model access via NOAA ARL READY website (http://ready. arl. noaa. gov/HYSPLIT. php). NOAA Air Resources Laboratory. Silver Spring, MD. 25, 2010.

Ehn, M., Thornton, J. A., Kleist, E., Sipila, M., Junninen, H., Pullinen, I., Springer, M., Rubach, F., Tillmann, R., Lee, B., Lopez-Hilfiker, F., Andres, S., Acir, I. H., Rissanen, M., Jokinen, T., Schobesberger, S., Kangasluoma, J., Kontkanen, J., Nieminen, T., Kurten, T., Nielsen, L. B., Jorgensen, S., Kjaergaard, H. G., Canagaratna, M., Maso, M. D., Berndt, T., Petaja, T., Wahner, A., Kerminen, V. M., Kulmala, M., Worsnop, D. R., Wildt, J., and Mentel, T. F.: A large source of low-volatility secondary organic aerosol, Nature., 506, 476-479, doi:10.1038/nature13032, 2014.

Elm, J., Fard, M., Bilde, M., and Mikkelsen, K. V.: Interaction of Glycine with Common Atmospheric Nucleation Precursors, J. Phys. Chem. A., 117, 12990-12997, doi:10.1021/jp408962c, 2013.

Ge, P., Luo, G., Luo, Y., Huang, W., Xie, H. B., Chen, J. W., and Qu, J. P.: Molecular understanding of the interaction of amino acids with sulfuric acid in the presence of water and the atmospheric implication, Chemosphere., 210, 215-223, doi:10.1016/j.chemosphere.2018.07.014, 2018.

Ge, X. L., Wexler, A. S., and Clegg, S. L.: Atmospheric amines – Part I. A review, Atmos. Environ., 45, 524-546, doi:10.1016/j.atmosenv.2010.10.012, 2011.

Gelin, F., Volkman, J. K., De Leeuw, J. W., and Sinninghe Damsté, J. S.: Mid-chain hydroxy long-chain fatty acids in microalgae from the genus Nannochloropsis, Phytochemistry., 45, 641-646, doi:10.1016/S0031-9422(97)00068-X, 1997.

Guo, Z. G., Sheng, L. F., Feng, J. L., and Fang, M.: Seasonal variation of solvent extractable organic compounds in the aerosols in Qingdao, China, Atmos. Environ., 37, 1825-1834, doi:10.1016/S1352-2310(03)00064-5, 2003.

Hao, Z. N., Yin, Y. G., Cao, D., and Liu, J. F.: Probing and Comparing the Photobromination and Photoiodination of Dissolved Organic Matter by Using Ultra-High-Resolution Mass Spectrometry, Environ. Sci. Technol., 51, 5464-5472, doi:10.1021/acs.est.6b03887, 2017.

675 Ishijima, H., Uchida, R., Ohtawa, M., Kondo, A., Nagai, K., Shima, K., Nonaka, K.,
676 Masuma, R., Iwamoto, S., Onodera, H., Nagamitsu, T., and Tomoda, H.:
677 Simplifungin and Valsafungins, Antifungal Antibiotics of Fungal Origin, J. Org.
678 Chem., 81, 7373-7383, doi:10.1021/acs.joc.6b00952, 2016.
679 Jares-Erijman, E. A., Bapat, C. P., Lithgow-Bertelloni, A., Rinehart, K. L., and Sakai,
680 R.: Crucigasterins, new polyunsaturated amino alcohols from the mediterranean
681 tunicate Pseudodistoma crucigaster, J. Org. Chem., 58, 5732-5737,
682 doi:10.1021/jo00073a036, 1993.
683 Jen, C. N., McMurry, P. H., and Hanson, D. R.: Stabilization of Sulfuric Acid Dimers
684 by Ammonia, Methylamine, Dimethylamine, and Trimethylamine, J. Geophys.
685 Res-Atmos., 119, 7502-7514, doi:10.1002/2014JD021592, 2014.
686 Jiang, B., Kuang, B. Y., Liang, Y. M., Zhang, J. Y., Huang, X. H. H., Xu, C. M., Yu, J.,
687 and Shi, Q.: Molecular composition of urban organic aerosols on clear and hazy
688 days in Beijing: A comparative study using FT-ICR MS, Environ. Chem., 13,
689 888-901, doi:10.1071/EN15230, 2016.
690 Kendel, M., Barnathan, G., Fleurence, J., Rabesaotra, V., and Wielgosz-Collin, G.:
691 Non-methylene Interrupted and Hydroxy Fatty Acids in Polar Lipids of the Alga
692 Grateloupia turuturu Over the Four Seasons, Lipids., 48, 535-545,
693 doi:10.1007/s11745-013-3783-5, 2013.
694 Kim, K. R., and Oh, D. K.: Production of hydroxy fatty acids by microbial fatty
695 acid-hydroxylation enzymes, Biotechnol. Adv., 31, 1473-1485,
696 doi:10.1016/j.biotechadv.2013.07.004, 2013.
697 Kourtchev, I., Fuller, S., Aalto, J., Ruuskanen, T. M., McLeod, M. W., Maenhaut, W.,
698 Jones, R., Kulmala, M., and Kalberer, M.: Molecular composition of boreal forest
699 aerosol from Hyytiala, Finland, using ultrahigh resolution mass spectrometry,
700 Environ. Sci. Technol., 47, 4069-4079, doi:10.1021/es3051636, 2013.
701 Kumar, M., Saiz-Lopez, A., and Francisco, J. S.: Single-Molecule Catalysis Revealed:
702 Elucidating the Mechanistic Framework for the Formation and Growth of
703 Atmospheric Iodine Oxide Aerosols in Gas-Phase and Aqueous Surface
704 Environments, J. Am. Chem. Soc., 140, 14704-14716, 10.1021/jacs.8b07441,
705 2018.
706 Kurtén, T., Loukonen, V., Vehkamäki, H., and Kulmala, M.: Amines are likely to
707 enhance neutral and ion-induced sulfuric acid-water nucleation in the atmosphere
708 more effectively than ammonia, Atmos. Chem. Phys., 8, 7455-7476,
709 doi:10.5194/acpd-8-7455-2008, 2008.
710 Li, D. F., Chen, D. P., Liu, F. Y., and Wang, W. L.: Role of glycine on sulfuric
711 acid-ammonia clusters formation: Transporter or participator, J. Environ. Sci. , 89,
712 125-135, doi:10.1016/j.jes.2019.10.009, 2020.
713 Lin, P., Rincon, A. G., Kalberer, M., and Yu, J. Z.: Elemental Composition of HULIS
714 in the Pearl River Delta Region, China: Results Inferred from Positive and Negative
715 Electrospray High Resolution Mass Spectrometric Data, Environ. Sci. Technol., 46,
716 7454-7462, doi:10.1021/es300285d, 2012.

Litchfield, C., Greenberg, A. J., Noto, G., and Morales, R. W.: Unusually high levels of C24−C30 fatty acids in sponges of the class demospongiae, Lipids., 11, 567-570, doi:10.1007/BF02532903, 1976.

Mahajan, A. S., Sorribas, M., Martín, J. C. G., MacDonald, S. M., Gil, M., Plane, J. M. C., and Saiz-Lopez, A.: Concurrent observations of atomic iodine, molecular iodine and ultrafine particles in a coastal environment, Atmos. Chem. Phys. Discuss., 11, 2545-2555, doi:10.5194/acp-11-2545-2011, 2010.

Mahajan, A. S., Plane, J. M. C., Oetjen, H., Mendes, L., Saunders, R. W., Saiz-Lopez, A., Jones, C. E., Carpenter, L. J., and McFiggans, G. B.: Measurement and modelling of tropospheric reactive halogen species over the tropical Atlantic Ocean, Atmos. Chem. Phys., 10, 4611–4624, doi: 10.5194/acp-10-4611-2010, 2010.

Mahajan, A. S., Martin, J. C. G., Hay, T. D., Royer, S. J., Yvon-Lewis, S., Liu, Y., Hu, L., Prados-Roman, C., Ordonez, C., Plane, J. M. C., and Saiz-Lopez, A.: Latitudinal distribution of reactive iodine in the Eastern Pacific and its link to open ocean sources, Atmos. Chem. Phys., 12, 11609-11617, 10.5194/acp-12-11609-2012, 2012.

Mansour, M. P., Volkman, J. K., Holdsworth, D. G., Jackson, A. E., and Blackburn, S. I.: Very-long-chain (C28) highly unsaturated fatty acids in marine dinoflagellates, Phytochemistry., 50, 541-548, doi:10.1016/S0031-9422(98)00564-0, 1999.

Mazzoleni, L. R., Saranjampour, P., Dalbec, M. M., Samburova, V., Hallar, G. A., Zielinska, B., Lowenthal, D. H., and Kohl, S.: Identification of water-soluble organic carbon in non-urban aerosols using ultrahigh-resolution FT-ICR mass spectrometry: Organic anions, Environ. Chem., 9, 285-297, doi:10.1071/EN11167, 2012.

Mäkelä, J. M., Hoffmann, T., Holzke, C., Väkevä, M., Suni, T., Mattila, T., Aalto, P. P., Tapper, U., Kauppinen, E. I., and O'Dowd, C. D., Biogenic iodine emissions and identification of end - products in coastal ultrafine particles during nucleation bursts, J. Geophys. Res., 107(D19), 8110, doi:10.1029/2001JD000580, 2002.

Mentel, T. F., Springer, M., Ehn, M., Kleist, E., Pullinen, I., Kurtén, T., Rissanen, M., Wahner, A., and Wildt, J.: Formation of highly oxidized multifunctional compounds: autoxidation of peroxy radicals formed in the ozonolysis of alkenes – deduced from structure–product relationships, Atmos. Chem. Phys., 15, 6745-6765, doi:10.5194/acp-15-6745-2015, 2015.

Merikanto, J., Spracklen, D. V., Mann, G. W., Pickering, S. J., and Carslaw, K. S.: Impact of nucleation on global CCN, Atmos. Chem. Phys., 9, 12999–13037, doi:10.5194/acp-9-8601-2009, 2009.

Metzger, A., Verheggen, B., Dommen, J., Duplissy, J., Prevot, A. S. H., Weingartner, E., Riipinen, I., Kulmala, M., Spracklen, D. V., Carslaw, K. S., and Baltensperger, U.: Evidence for the role of organics in aerosol particle formation under atmospheric conditions, Proc. Natl. Acad. Sci. U. S. A., 107, 6646-6651, doi:10.1073/pnas.0911330107, 2010.

Moss, G. P., Smith, P. A. S., and Tavernier, D.: Glossary of class names of organic compounds and reactivity intermediates based on structure (IUPAC

760 Recommendations 1995), pac, 67, 1307-1375, doi:10.1351/pac199567081307,
761 1995.
762 Ning, C. P., Gao, Y., Zhang, H. J., Yu, H. R., Wang, L., Geng, N. B., Cao, R., and
763 Chen, J. P.: Molecular characterization of dissolved organic matters in winter
764 atmospheric fine particulate matters (PM2.5) from a coastal city of northeast China,
765 Sci. Total. Environ., 689, 312-321, doi:10.1016/j.scitotenv.2019.06.418, 2019.
766 O'Dowd, C. D., Jimenez, J. L., Bahreini, R., Flagan, R. C., Seinfeld, J. H., Hämeri, K.,
767 Pirjola, L., Kulmala, M., Jennings, S. G., and Hoffmann, T.: Marine aerosol
768 formation from biogenic iodine emissions, Nature., 417, 632-636,
769 doi:10.1038/nature00775, 2002.
770 Pankow, J. F., and Asher, W. E.: SIMPOL.1: a simple group contribution method for
771 predicting vapor pressures and enthalpies of vaporization of multifunctional
772 organic compounds, Atmos. Chem. Phys., 8, 2773-2796,
773 doi:10.5194/acp-8-2773-2008, 2008.
774 Pollard, M., Beisson, F., Li, Y., and Ohlrogge, J. B.: Building lipid barriers:
775 biosynthesis of cutin and suberin, Trends. Plant. Sci., 13, 236-246,
776 doi:10.1016/j.tplants.2008.03.003, 2008.
777 Perämäkylä, O., Riva, M., Heikkinen, L., Quéléver, L., Roldin, P., and Ehn, M.:
778 Experimental investigation into the volatilities of highly oxygenated organic
779 molecules (HOMs) , Atmos. Chem. Phys., 20, 649–669,
780 doi:10.5194/acp-2019-620, 2020.
781 Pospisilova, V., Lopez-Hilfiker, F. D., Bell, D. M., El Haddad, I., Mohr, C., Huang,
782 W., Heikkinen, L., Xiao, M., Dommen, J., Prevot, A. S. H., Baltensperger, U., &
783 Slowik, J. G.: On the fate of oxygenated organic molecules in atmospheric aerosol
784 particles. Science Advances, 6(11), 1–12., doi: 10.1126/sciadv.aax8922, 2020.
785 Pratt, K. A., and Prather, K. A.: Mass spectrometry of atmospheric aerosols--recent
786 developments and applications. Part I: Off-line mass spectrometry techniques,
787 Mass. Spectrom. Rev., 31, 1-16, doi:10.1002/mas.20322, 2012.
788 Quinn, P. K., Bates, T. S., Schulz, K. S., Coffman, D. J., Frossard, A. A., Russell, L.
789 M., Keene, W. C., and Kieber, D. J.: Contribution of sea surface carbon pool to
790 organic matter enrichment in sea spray aerosol, Nat. Geosci., 7, 228-232,
791 doi:10.1038/ngeo2092, 2014.
792 Řezanka, T., and Podojil, M.: The very long chain fatty acids of the green
793 alga,Chlorella kessleri, Lipids., 19, 472, doi:10.1007/BF02537412, 1984.
794 Richters, S., Herrmann, H., and Berndt, T.: Highly Oxidized RO2 Radicals and
795 Consecutive Products from the Ozonolysis of Three Sesquiterpenes, Environ. Sci.
796 Technol., 50, 2354-2362, doi:10.1021/acs.est.5b05321, 2016.
797 Rogge, W. F., Hildemann, L. M., Mazurek, M. A., Cass, G. R., and Simoneit, B. R. T.:
798 Sources of fine organic aerosol. 1. Charbroilers and meat cooking operations,
799 Environ. Sci. Technol., 25, 1112-1125, doi:10.1021/es00018a015, 1991.
800 Roscoe, H. K., Jones, A. E., Brough, N., Weller, R., Saiz-Lopez, A., Mahajan, A. S.,
801 Schoenhardt, A., Burrows, J. P., and Fleming, Z. L.: Particles and iodine
802 compounds in coastal Antarctica, J. Geophys. Res-Atmos., 120, 7144-7156,
803 doi:10.1002/2015JD023301, 2015.

Russell, L. M., Hawkins, L. N., Frossard, A. A., Quinn, P. K., and Bates, T. S.: Carbohydrate-like composition of submicron atmospheric particles and their production from ocean bubble bursting, Proc. Natl. Acad. Sci. U. S. A., 107, 6652, doi:10.1073/pnas.0908905107, 2010.

Saiz-Lopez, A., and Plane, J. M. C.: Novel iodine chemistry in the marine boundary layer, Geophys. Res. Lett., 31, L04112, doi:10.1029/2003GL019215, 2004.

Saiz-Lopez, A., Plane, J. M. C., Baker, A. R., Carpenter, L. J., von Glasow, R., Gómez Martín, J. C., McFiggans, G., and Saunders, R. W.: Atmospheric Chemistry of Iodine, Chem. Rev., 112, 1773-1804, doi:10.1021/cr200029u, 2012.

Schervish, M., and Donahue, N. M.: Peroxy Radical Chemistry and the Volatility Basis Set. Atmos. Chem. Phys., 20, 1183–1199, doi: 10.5194/acp-20-1183-2020, 2020.

Schmitt-Kopplin, P., Liger-Belair, G., Koch, B. P., Flerus, R., Kattner, G., Harir, M., Kanawati, B., Lucio, M., Tziotis, D., Hertkorn, N., and Gebefügi, I.: Dissolved organic matter in sea spray: a transfer study from marine surface water to aerosols, Biogeosciences., 9, 1571-1582, doi:10.5194/bg-9-1571-2012, 2012.

Schum, S. K., Zhang, B., Džepina, K., Fialho, P., Mazzoleni, C., and Mazzoleni, L. R.: Molecular and physical characteristics of aerosol at a remote free troposphere site: implications for atmospheric aging, Atmos. Chem. Phys., 18, 14017-14036, doi:10.5194/acp-18-14017-2018, 2018.

Simon, M., Dada, L., Heinritzi, M., Scholz, W., Stolzenburg, D., Wagner, A. C., Kürten, A., Rörup, B., He, X., Almeida, J., Baccarini, A., Bauer, P. S., Beck, L., Bergen, A., Bianchi, F. et al.: Molecular understanding of new-particle formation from alpha-pinene between −50 °C and 25 °C, Atmos. Chem. Phys. Discuss., https://doi.org/10.5194/acp-2019-1058, in review, 2020.

Simoneit, B. R. T., and Mazurek, M. A.: Organic matter of the troposphere—II.**For Part I, see Simoneit et al. (1977). Natural background of biogenic lipid matter in aerosols over the rural western united states, Atmos. Environ., 16, 2139-2159, doi:10.1016/0004-6981(82)90284-0, 1982.

Sipilä, M., Sarnela, N., Jokinen, T., Henschel, H., Junninen, H., Kontkanen, J., Richters, S., Kangasluoma, J., Franchin, A., Peräkylä, O., Rissanen, M. P., Ehn, M., Vehkamäki, H., Kurten, T., Berndt, T., Petäjä, T., Worsnop, D., Ceburnis, D., Kerminen, V.-M., Kulmala, M., and O'Dowd, C.: Molecular-scale evidence of aerosol particle formation via sequential addition of HIO3, Nature., 537, 532-534, doi:10.1038/nature19314, 2016.

Stevanović, K. Z., Bubanja, I. N. M., and Stanisavljev, D. R.: Is Iodine Oxidation with Hydrogen Peroxide Coupled with Nucleation Processes?, J. Phys. Chem. C., 123, 16671-16680, doi:10.1021/acs.jpcc.9b02563, 2019.

Tsukamoto, D., Shibano, M., and Kusano, G.: Studies on the Constituents of Broussonetia Species X. Six New Alkaloids from Broussonetia kazinoki SIEB, Chem. Pharm. Bull., 49, 1487-1491, doi:10.1248/cpb.49.1487, 2001.

Vaattovaara, P., Huttunen, P. E., Yoon, Y. J., Joutsensaari, J., Lehtinen, K. E. J., O'Dowd, C. D., and Laaksonen, A.: The composition of nucleation and Aitken modes particles during coastal nucleation events: evidence for marine secondary

organic contribution, Atmos. Chem. Phys., 6, 4601–4616, doi: 10.5194/acp-6-4601-2006, 2006.
VanMiddlesworth, F., Giacobbe, R. A., Lopez, M., Garrity, G., Bland, J., Bartizal, K., Fromtling, R. A., Polishook, J., Zweerink, M., and Edison, A. M.: Sphingofungins A, B, C, and D; a new family of antifungal agents. I. Fermentation, isolation, and biological activity, J. Antibiot., 45, 861-867, 1992.
Vereecken, L., Glowacki, D. R., and Pilling, M. J.: Theoretical Chemical Kinetics in Tropospheric Chemistry: Methodologies and Applications, Chem. Rev., 115, 4063-4114, doi:10.1021/cr500488p, 2015.
Volkman, J. K., Barrett, S. M., Dunstan, G. A., and Jeffrey, S. W.: C30-C32 alkyl diols and unsaturated alcohols in microalgae of the class Eustigmatophyceae, Org. Geochem., 18, 131-138, doi:10.1016/0146-6380(92)90150-V, 1992.
Wang, Y., Riva, M., Xie, H., Heikkinen, L., Schallhart, S., Zha, Q., Yan, C., He, X., Perä kylä, O., and Ehn, M.: Formation of highly oxygenated organic molecules from chlorine atom initiated oxidation of alpha-pinene. Atmospheric Chemistry and Physics, 20, 5145–5155. doi:10.5194/acp-2019-807, 2020.
Willoughby, A. S., Wozniak, A. S., and Hatcher, P. G.: Detailed Source-Specific Molecular Composition of Ambient Aerosol Organic Matter Using Ultrahigh Resolution Mass Spectrometry and 1H NMR, Atmosphere., 7, 79, doi:10.3390/atmos7060079, 2016.
Wilson, T. W., Ladino, L. A., Alpert, P. A., Breckels, M. N., Brooks, I. M., Browse, J., Burrows, S. M., Carslaw, K. S., Huffman, J. A., Judd, C., Kilthau, W. P., Mason, R. H., McFiggans, G., Miller, L. A., Nájera, J. J., Polishchuk, E., Rae, S., Schiller, C. L., Si, M., Temprado, J. V., Whale, T. F., Wong, J. P. S., Wurl, O., Yakobi-Hancock, J. D., Abbatt, J. P. D., Aller, J. Y., Bertram, A. K., Knopf, D. A., and Murray, B. J.: A marine biogenic source of atmospheric ice-nucleating particles, Nature., 525, 234-238, doi:10.1038/nature14986, 2015.
Wu, C. H., Yang, J., Fu, Q., Zhu, B., Ruan, T., and Jiang, G. B.: Molecular characterization of water-soluble organic compounds in PM2.5 using ultrahigh resolution mass spectrometry, Sci. Total. Environ., 668, 917-924, doi:10.1016/j.scitotenv.2019.03.031, 2019.
Xie, Q. R., Su, S. H., Chen, S., Xu, Y. S., Cao, D., Chen, J., Ren, L. J., Yue, S. Y., Zhao, W. Y., Sun, Y. L., Wang, Z. F., Tong, H. J., Su, H., Cheng, Y. F., Kawamura, K., Jiang, G. B., Liu, C. Q., and Fu, P. Q.: Molecular Characterization of Firework-Related Urban Aerosols using FT-ICR Mass Spectrometry, Atmos. Chem. Phys. , 1-29, doi: 10.5194/acp-2019-1180, 2020.
Yang, Y. J., Peng, Y. E., Chang, Q., Dan, C. H., Guo, W., and Wang, Y. X.: Selective Identification of Organic Iodine Compounds Using Liquid Chromatography–High Resolution Mass Spectrometry, Anal. Chem., 88, 1275-1280, doi:10.1021/acs.analchem.5b03694, 2016.
Yao, L., Wang, M. Y., Wang, X. K., Liu, Y. J., Chen, H. F., Zheng, J., Nie, W., Ding, A. J., Geng, F. H., Wang, D. F., Chen, J. M., Worsnop, D. R., and Wang, L.: Detection of atmospheric gaseous amines and amides by a high-resolution time-of-flight chemical ionization mass spectrometer with protonated ethanol

reagent ions, Atmos. Chem. Phys., 16, 14527-14543, doi:10.5194/acp-16-14527-2016, 2016.
Yassine, M. M., Harir, M., Dabek, E., and Schmitt-Kopplin, P.: Structural characterization of organic aerosol using Fourier transform ion cyclotron resonance mass spectrometry: Aromaticity equivalent approach, Rapid. Commun. Mass. Sp., 28, 2445-2454, doi:10.1002/rcm.7038, 2014.
Yoon, Y. J., O'Dowd, C. D., Jennings, S. G., and Lee, S. H.: Statistical characteristics and predictability of particle formation events at Mace Head, J. Geophys. Res., 111, D13204, doi:10.1029/2005JD006284, 2006.
Yu, H., Ren, L. L., Huang, X. P., Xie, M. J., He, J., and Xiao, H.: Iodine speciation and size distribution in ambient aerosols at a coastal new particle formation hotspot in China, Atmos. Chem. Phys., 19, 4025-4039, doi:10.5194/acp-19-4025-2019, 2019.
Yvon, S. A., Saltzman, E. S., Cooper, D. J., Bates, T. S., and Thompson, A. M.: Atmospheric sulfur cycling in the tropical Pacific marine boundary layer (12 ℃S, 135 ℃W): A comparison of field data and model results: 1. Dimethylsulfide, J. Geophys. Res-Atmos., 101, 6899-6909, doi:10.1029/95JD03356, 1996.
Zhao, R., Kenseth, C. M., Huang, Y., Dalleska, N. F., Kuang, X. M., Chen, J., Paulson, S. E., & Seinfeld, J. H.: Rapid Aqueous-Phase Hydrolysis of Ester Hydroperoxides Arising from Criegee Intermediates and Organic Acids. Journal of Physical Chemistry A, 122(23), 5190–5201. doi: 10.1021/acs.jpca.8b02195, 2018.
Zhao, R.; Kenseth, C. M.; Huang, Y.; Dalleska, N. F.; Seinfeld, J. H. Iodometry-assisted liquid chromatography electrospray ionization mass spectrometry for analysis of organic peroxides - an application to atmospheric secondary organic aerosol. Environ. Sci. Technol. 2018, 52, 2108−2117.
Zhao, Y., Hallar, A. G., and Mazzoleni, L. R.: Atmospheric organic matter in clouds: exact masses and molecular formula identification using ultrahigh-resolution FT-ICR mass spectrometry, Atmos. Chem. Phys., 13, 12343-12362, doi:10.5194/acp-13-12343-2013, 2013.
Zheng, M., Fang, M., Wang, F., and To, K. L.: Characterization of the solvent extractable organic compounds in PM2.5 aerosols in Hong Kong, Atmos. Environ., 34, 2691-2702, doi:10.1016/S1352-2310(99)00521-X, 2000.
Zuth, C., Vogel, A. L., Ockenfeld, S., Huesmann, R., and Hoffmann, T.: Ultrahigh-Resolution Mass Spectrometry in Real Time: Atmospheric Pressure Chemical Ionization Orbitrap Mass Spectrometry of Atmospheric Organic Aerosol, Anal. Chem., 90, 8816-8823, doi:10.1021/acs.analchem.8b00671, 2018.

Supporting Information

Probing key organic substances driving new particle growth initiated by iodine nucleation in coastal atmosphere

Yibei Wan,[1] Xiangpeng Huang,[2] Bin Jiang,[3] Binyu Kuang,[4] Manfei Lin,[4] Deming Xia[5], Yuhong Liao,[3] Jingwen Chen,[5] Jianzhen Yu,[4] and Huan Yu[1]

[1] Department of Atmospheric Science, School of Environmental Studies, China University of Geosciences, Wuhan, 430074, China

[2] School of Environmental Science and Engineering, Nanjing University of Information Science and Technology, Nanjing, 210044, China

[3] Guangzhou Institute of Geochemistry, Chinese Academy of Sciences, Guangzhou 510640, China

[4] Department of Chemistry, Hong Kong University of Science & Technology, Clear Water Bay, Kowloon, Hong Kong, China

[5] School of Environmental Science and Technology, Dalian University of Technology, Dalian 116024, China

Corresponding author: H. Yu (yuhuan@cug.edu.cn)

Text:

ESI-FT-ICR MS operation conditions

Figures:

Figure S1: Figure S1. (a) The observation site, indicated as a red star, in an aerial photograph. Photo source: Baidu Map. (b) 72-hour air mass back trajectories ending at 100 m above ground level at the observation site computed by HYSPLIT model during the I-NPF events from May 8 to 10, 2018.

Figure S2. (a), (c) Number concentration of 2-7 nm particles ($N_{2\text{-}7}$), tidal height and solar radiation intensity during the Iodine-initiated NPF (I-NPF) days from May 9 to 11 and the continental regional NPF (C-NPF) days from February 11 to 13. Particle number size distribution and 10-56 nm particle mass concentration during (b) I-NPF days from May 9 to 11, (d) C-NPF days from February 11 to 13 and (e) non-NPF days from April 16 to 18.

Figure S3. Reconstructed mass spectra of the 7 elemental groups in ESI-and ESI+ modes for the four size bins.

Figure S4: DBE vs. C atom number diagrams of all the CHON and CHO formulas detected in 10–18 nm particles in ESI+ mode. (a) (b) +H adducts, (c) (d) +Na adducts. The color bar denotes the O number in the formulas. The size of the circles reflects the relative intensities of molecular formulas on a logarithmic scale.

Figure S5: Relative intensities of subgroups according to O atom number in CHON, CHO, CHONI and CHOI formulas in the four size bins in ESI+ (in red) and ESI- (in blue). The intensity of the most abundant subgroup is defined as 1 and those of other subgroups are normalized by it. The relative intensities of non-iodinated OC formulas (iodinated OC formulas) are plotted in the region above (below) zero line.

Figure S6: O atom number of *vs.* N atom number of $C_{10}H_xO_yN_z$ compounds detected in 180–560 nm particles (a) and $C_{18}H_xO_yN_z$ compounds detected in 10–18 nm particles in ESI- mode (b).

Figure S7: Simplified reaction scheme showing the formation of oxygenated and nitrated CHO and CHON compounds from α-linolenic acid oxidation in the atmosphere.

Figure S8: Simplified reaction scheme showing the formation of oxygenated CHO compounds from unsaturated C_{28} FA ($C_{28}H_{52}O_2$) oxidation in the atmosphere.

Figure S9: Simplified reaction scheme showing the formation of oxygenated CHON compounds containing a $–NH_2$ group from unsaturated C_{18} amino alcohol ($C_{18}H_{37}NO_4$) oxidation in the atmosphere.

Tables:

Table S1. Predicted saturation concentration (C*) range of most abundant CHON and CHO formulas, as well as their possible precursors.

ESI-FT-ICR MS operation conditions

A syringe pump infused the sample extract continuously into the ESI unit with a flow rate of 180 μL h-1. The ESI source conditions were as follows: the nebulizer gas pressure was 1 bar; the dry gas (N_2) pressure was 4 bar and its temperature was 200 ℃; the capillary voltage was 4.5 kV. The ion accumulation time in the argon-filled hexapole collision pool with 1.5 V of direct current voltage and 1400 Vp-p of radio frequency (RF) amplitude was 0.05 s, followed by transport ions through a hexapole ion guide to the ICR cell for 0.7 ms. 4 M words of data were recorded over the mass range of 150-1000 Da for each run. A total of 128 scans were collected to enhance the signal/noise (S/N) ratio and dynamic range.

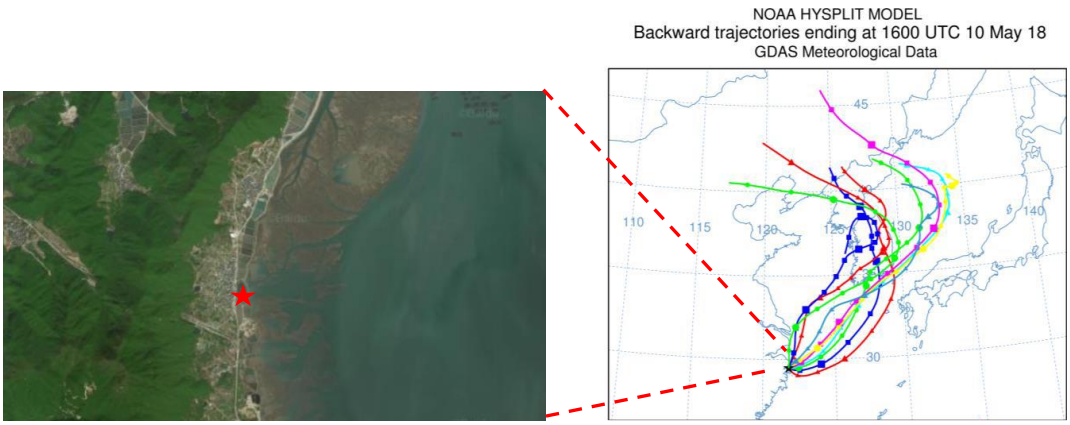

Figure S1. (a) The observation site, indicated as a red star, in an aerial photograph. Photo source: Baidu Map. (b) 72-hour air mass back trajectories ending at 100 m above ground level at the observation site computed by HYSPLIT model during the I-NPF events from May 8 to 10, 2018.

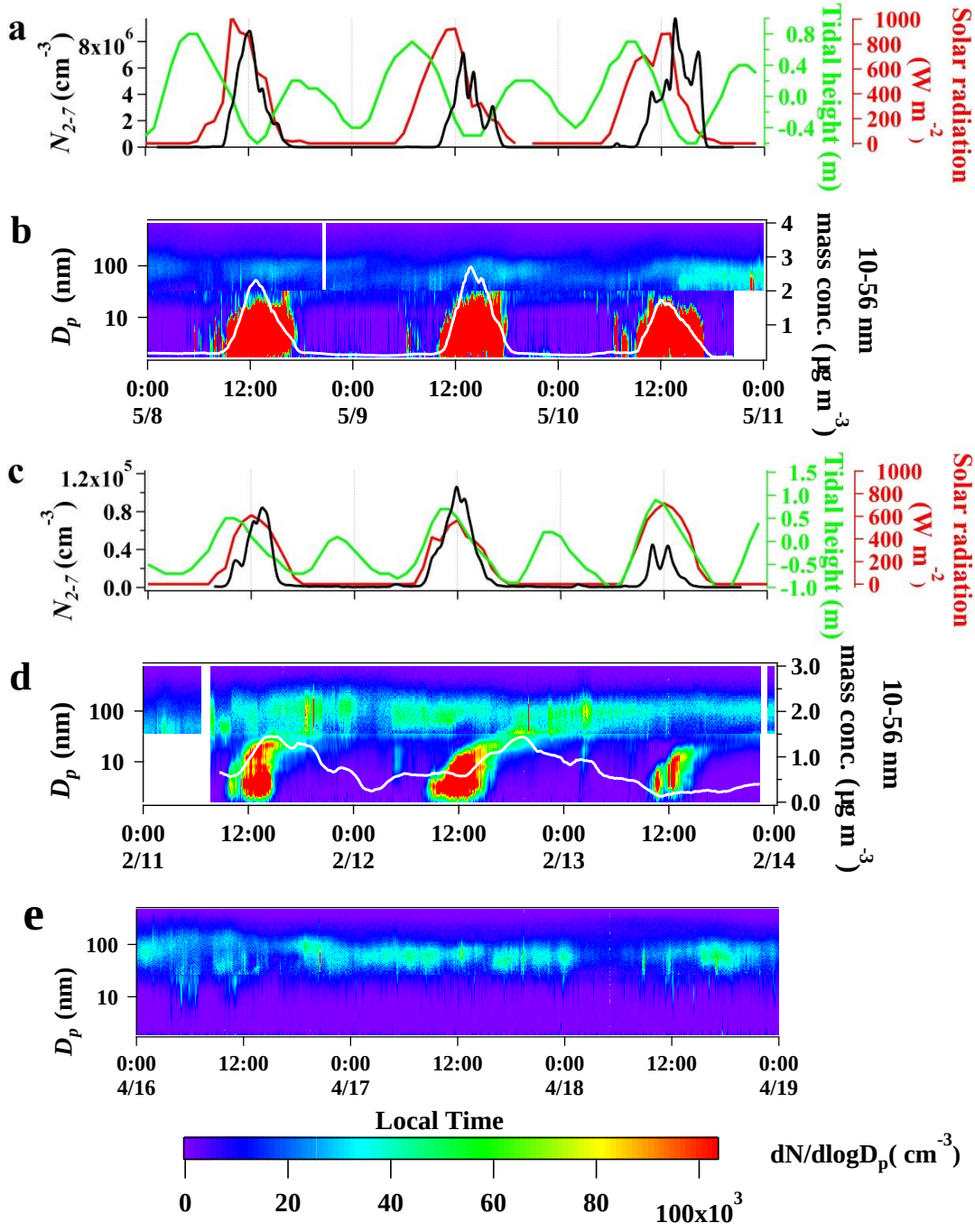
a
N_{2-7} (cm^{-3})
8x10^6
6
4
2
0
Tidal height (m)
0.8
0.4
0.0
-0.4
Solar radiation
(W m^{-2})
1000
800
600
400
200
0
b
D_p (nm)
100
10
mass conc. (μg m^{-3})
4
3
2
1
10-56 nm
0:00 5/8
12:00
0:00 5/9
12:00
0:00 5/10
12:00
0:00 5/11
c
N_{2-7} (cm^{-3})
1.2x10^5
0.8
0.4
0.0
Tidal height (m)
1.5
1.0
0.5
0.0
-0.5
-1.0
Solar radiation
(W m^{-2})
1000
800
600
400
200
0
d
D_p (nm)
100
10
mass conc. (μg m^{-3})
3.0
2.0
1.0
0.0
10-56 nm
0:00 2/11
12:00
0:00 2/12
12:00
0:00 2/13
12:00
0:00 2/14
e
D_p (nm)
100
10
0:00 4/16
12:00
0:00 4/17
12:00
0:00 4/18
12:00
0:00 4/19
Local Time
0
20
40
60
80
100x10^3
dN/dlogD$_p$(cm^{-3})

Figure S2. (a), (c) Number concentration of 2-7 nm particles ($N_{2\text{-}7}$), tidal height and solar radiation intensity during the Iodine-initiated NPF (I-NPF) days from May 9 to 11 and the continental regional NPF (C-NPF) days from February 11 to 13. Particle number size distribution and 10-56 nm particle mass concentration during (b) I-NPF days from May 9 to 11, (d) C-NPF days from February 11 to 13 and (e) non-NPF days from April 16 to 18.

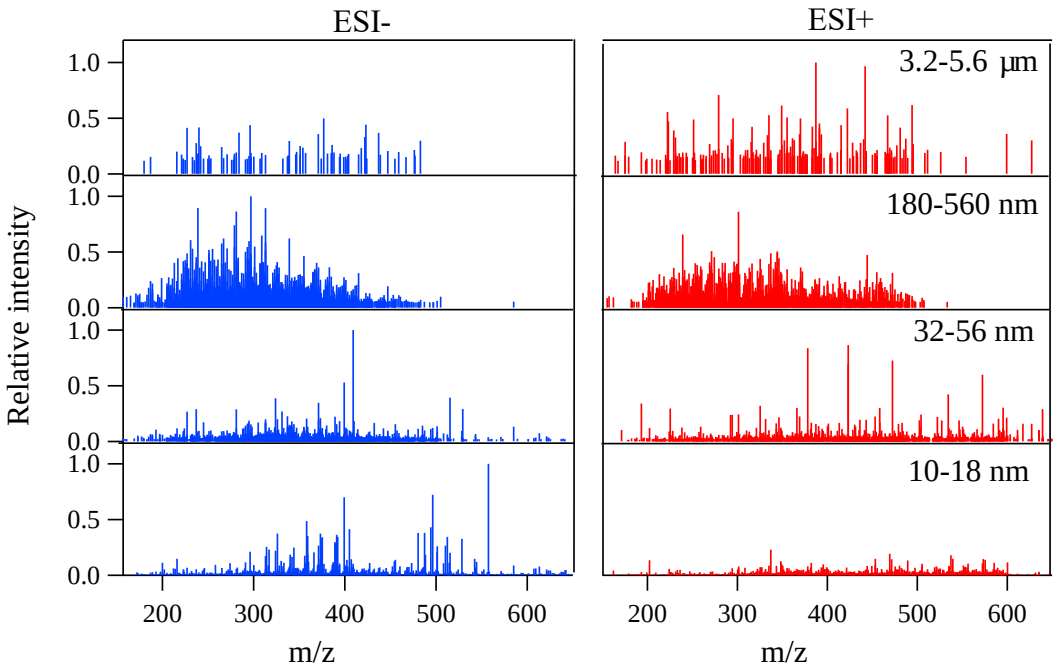

Figure S3. Reconstructed mass spectra of the 7 elemental groups in ESI- (left panels) and ESI+ (right panels) modes for the four size bins. The signals are normalized against the intensity of the most abundant molecular ions in a size bin.

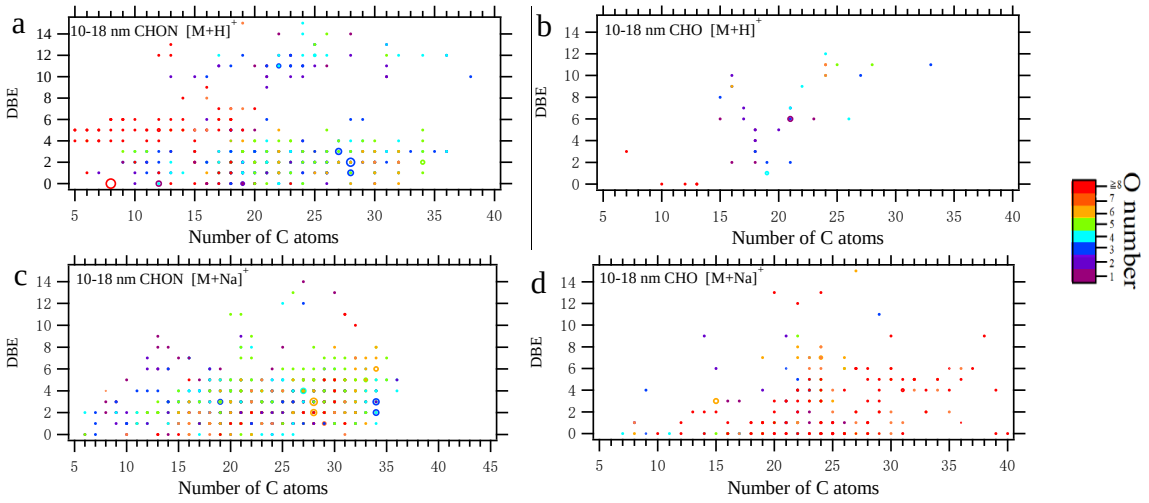

Figure S4. DBE vs. C atom number diagrams of all CHON and CHO formulas detected in 10–18 nm particles in ESI+ mode. (a) (b) $[M+H]^+$ adducts, (c) (d) $[M+Na]^+$ adducts. The color bar denotes O number in the formulas. The size of the circles reflects the relative intensities of molecular formulas on a logarithmic scale.

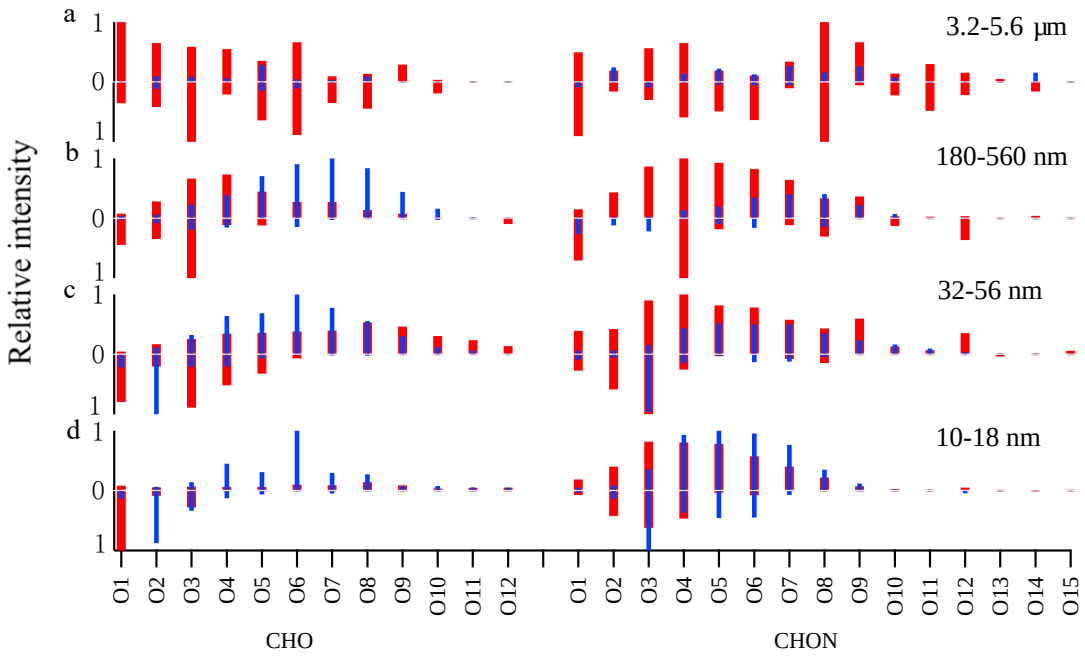

Figure S5. Relative intensities of subgroups according to O atom number in CHON, CHO, CHONI and CHOI formulas in the four size bins in ESI+ (in red) and ESI- (in blue). The intensity of the most abundant subgroup in a size bin is defined as 1 and those of other subgroups are normalized by it. The relative intensities of non-iodinated OC formulas (iodinated OC formulas) are plotted in the region above (below) zero line.

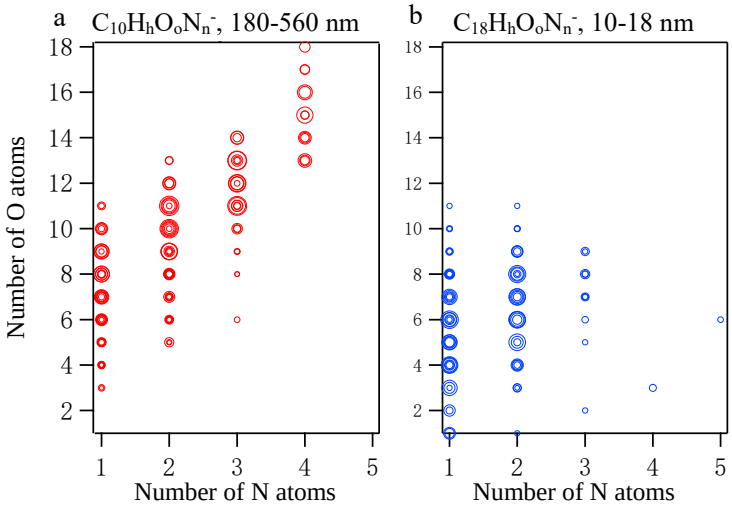

Figure S6. O atom number of *vs.* N atom number of $C_{10}H_hO_oN_n^-$ compounds detected in 180–560 nm particles (a) and $C_{18}H_hO_oN_n$- compounds detected in 10–18 nm particles in ESI- mode (b).

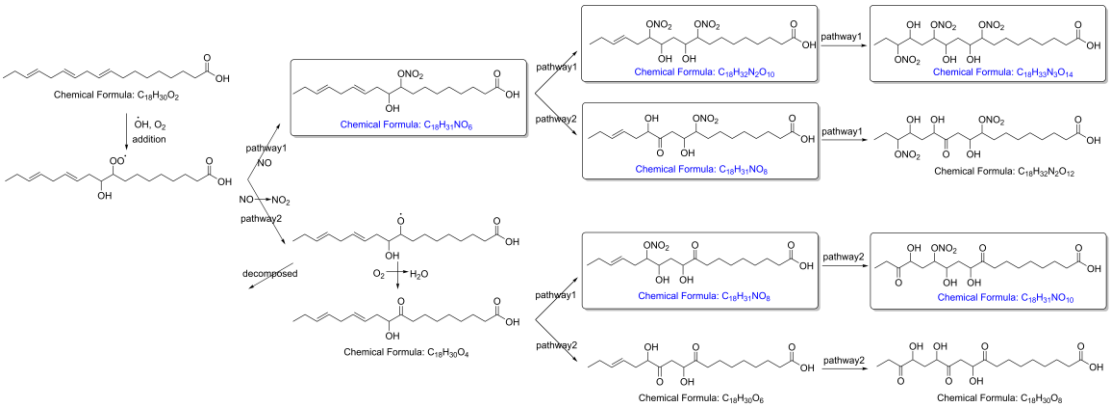

Figure S7. Simplified reaction scheme of the formation of oxygenated and nitrated CHO and CHON compounds from α-linolenic acid ($C_{18}H_{30}O_2$) oxidation in the atmosphere. One representative structure is shown for each chemical formula. Chemical formulas in the boxes are found in the formula list detected in 10–18 nm particles. Pathway 1: OH and O_2 addition followed by reaction with NO to form a –ONO_2 group; pathway 2: OH and O_2 addition followed by reaction with NO to form an alkoxy radical that further reacts with O_2 to form a –C=O group.

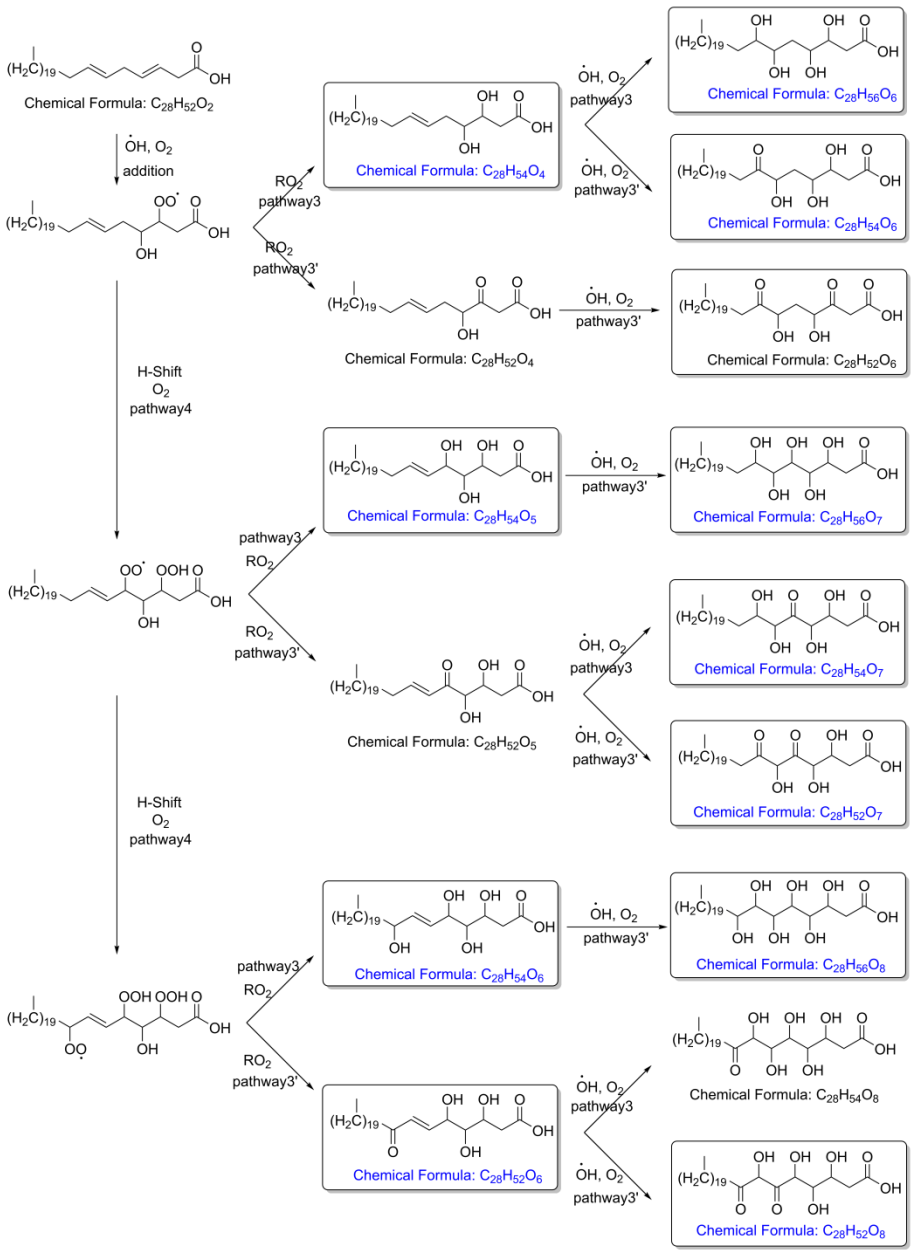

Figure S8. Simplified reaction scheme of the formation of oxygenated CHO compounds from unsaturated C_{28} FA ($C_{28}H_{52}O_2$) oxidation in the atmosphere. One representative structure is shown for each chemical formula. Chemical formulas in the boxes are found in the formula list detected in 10–18 nm particles. Pathway 3: OH and O_2 addition followed by reaction with RO_2 to form a –OH or a –C=O group; Pathway 4: successive intermolecular H-shift/O_2 addition (autoxidation) to form RO_2 radicals with –OOH group. –OOH group is not stable and decomposed to -OH.

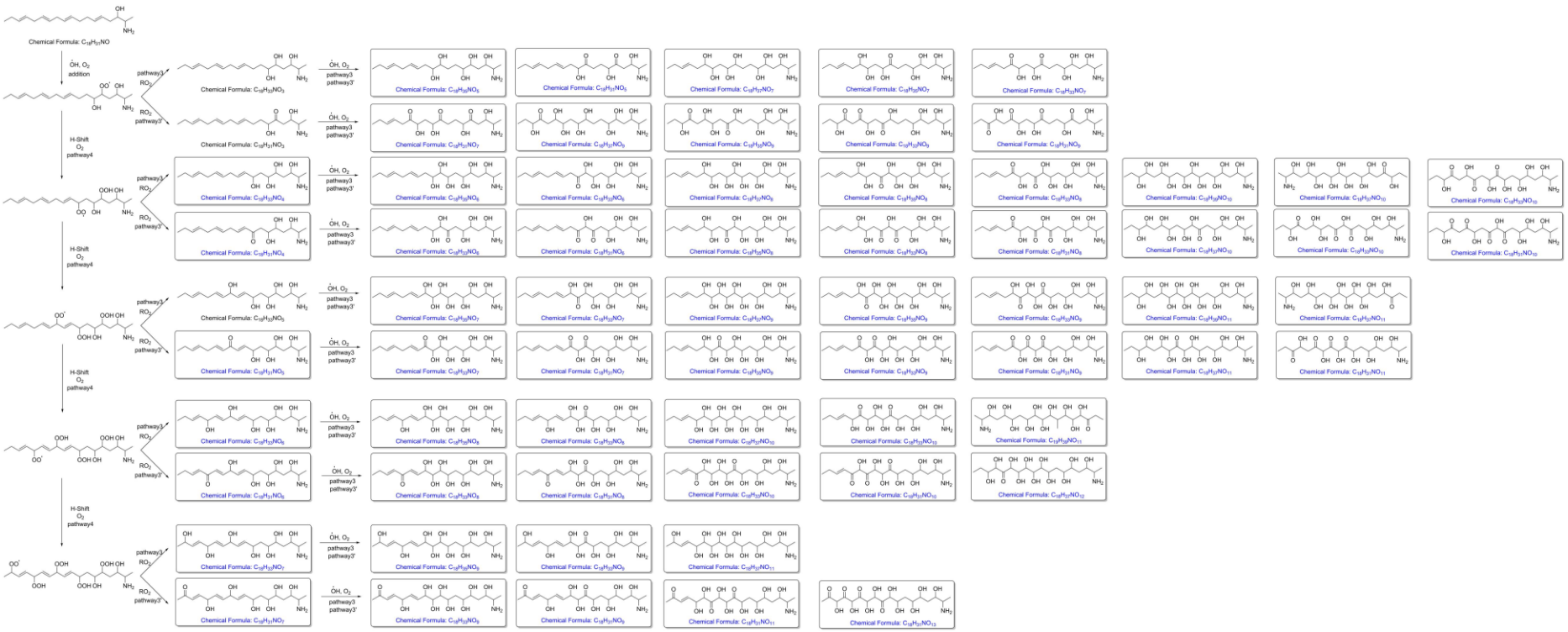

Figure S9. Simplified reaction scheme of the formation of oxygenated CHON compounds containing a $–NH_2$ group from unsaturated C_{18} amino alcohol ($C_{18}H_{37}NO_4$) oxidation in the atmosphere. One representative structure is shown for each chemical formula. Chemical formulas in the boxes are found in the formula list detected in 10–18 nm particles. Pathway 3: OH and O_2 addition followed by reaction with RO_2 to form a –OH or a –C=O group; Pathway 4: successive intermolecular H-shift/O_2 addition autoxidation to form RO_2 radicals with –OOH group.

Table S1. Predicted saturation concentration (C*) range of most abundant CHON and CHO formulas, as well as their possible precursors.

Formula	Predicted C^* ($\mu g\ m^{-3}$)	Predicted C^* of possible precursors ($\mu g\ m^{-3}$)
	ESI- mode	
$C_{18}H_{33}NO_4$	1.62×10^{-5}–2.06×10^{-2}	3.40×10^{-1}–8.91
$C_{18}H_{33}NO_6$	7.66×10^{-10}–1.33×10^{-2}	3.40×10^{-1}–8.87×10^{1}
$C_{18}H_{34}N_2O_6$	7.62×10^{-11}–1.32×10^{-3}	3.40×10^{-2}–8.91
$C_{18}H_{34}N_2O_7$	5.21×10^{-13}–9.06×10^{-6}	3.40×10^{-2}–8.91
$C_{18}H_{34}N_2O_8$	1.30×10^{-15}–5.56×10^{-6}	3.40×10^{-2}–8.91
$C_{18}H_{36}N_2O_5$	1.44×10^{-8}–1.10×10^{-2}	3.40×10^{-2}–8.87×10^{1}
$C_{18}H_{36}N_2O_6$	9.83×10^{-11}–7.54×10^{-5}	3.40×10^{-2}–8.87×10^{1}
$C_{18}H_{36}N_2O_7$	6.72×10^{-13}–5.15×10^{-7}	3.40×10^{-2}–8.87×10^{1}
$C_{19}H_{39}NO_7$	3.40×10^{-12}–1.15×10^{-7}	1.34×10^{-1}–3.51×10^{1}
$C_{30}H_{57}NO_4$	7.44×10^{-8}–6.69×10^{-6}	4.29×10^{-6}–1.16×10^{-3}
$C_{30}H_{59}NO_3$	5.58×10^{-9}–1.58×10^{-6}	4.29×10^{-6}–1.14×10^{-4}
$C_{30}H_{59}NO_4$	6.28×10^{-10}–8.62×10^{-6}	4.29×10^{-6}–1.16×10^{-3}
$C_{30}H_{59}NO_5$	4.52×10^{-12}–1.32×10^{-6}	4.29×10^{-6}–1.16×10^{-3}
$C_{30}H_{59}NO_6$	2.64×10^{-13}–8.93×10^{-9}	4.29×10^{-6}–1.16×10^{-3}
$C_{30}H_{60}O_6$	1.66×10^{-14}–3.76×10^{-13}	4.36×10^{-5}–1.16×10^{-3}
$C_{20}H_{40}O_6$	2.13×10^{-10}–4.83×10^{-9}	5.28×10^{-1}–1.39×10^{1}
$C_{21}H_{42}O_6$	8.32×10^{-11}–1.88×10^{-9}	2.07×10^{-1}–5.46×10^{0}
$C_{22}H_{44}O_4$	6.95×10^{-7}–1.57×10^{-5}	8.15×10^{-2}–2.15×10^{0}
$C_{24}H_{48}O_4$	1.06×10^{-7}–2.39×10^{-6}	1.25×10^{-2}–3.3×10^{-1}
$C_{26}H_{52}O_4$	1.60×10^{-8}–3.63×10^{-7}	1.90×10^{-3}–5.05×10^{-2}
$C_{27}H_{54}O_6$	2.87×10^{-13}–6.49×10^{-12}	7.42×10^{-4}–1.97×10^{-2}
$C_{28}H_{56}O_4$	2.41×10^{-9}–5.47×10^{-8}	2.89×10^{-4}–7.67×10^{-3}
$C_{28}H_{56}O_6$	1.11×10^{-13}–2.51×10^{-12}	2.89×10^{-4}–7.67×10^{-3}
$C_{29}H_{58}O_6$	4.29×10^{-14}–9.73×10^{-13}	1.12×10^{-4}–2.98×10^{-3}
$C_{33}H_{66}O_6$	9.56×10^{-16}–2.17×10^{-14}	2.54×10^{-6}–6.77×10^{-5}
$C_{38}H_{76}O_8$	3.66×10^{-22}–8.30×10^{-21}	2.18×10^{-8}–5.85×10^{-7}
	ESI+ mode	
$C_{11}H_{18}N_4O_8$	4.73×10^{-9}–3.63×10^{-3}	2.21×10^{0}–5.61×10^{2}
$C_{12}H_{20}N_4O_8$	1.85×10^{-9}–1.42×10^{-3}	8.85×10^{-1}–2.26×10^{2}
$C_{19}H_{35}NO_3$	9.26×10^{-4}	1.34×10^{-1}–2.23×10^{-1}
$C_{19}H_{36}N_2O_5$	4.35×10^{-9}–3.34×10^{-3}	1.34×10^{-1}–3.52×10^{0}
$C_{19}H_{37}NO_3$	1.20×10^{-3}–2.71×10^{-2}	1.34×10^{-1}–2.23×10^{-1}

$C_{19}H_{38}N_2O_3$	2.71×10^{-3}–5.04×10^{-3}	1.34×10^{-2}–3.52×10^{0}
$C_{24}H_{46}N_2O_4$	5.73×10^{-9}–4.39×10^{-3}	1.24×10^{-4}–3.28×10^{-2}
$C_{25}H_{43}NO_4$	3.07×10^{-7}–1.72×10^{-5}	4.83×10^{-4}–1.28×10^{-2}
$C_{26}H_{51}NO_5$	1.73×10^{-9}	1.88×10^{-4}–3.13×10^{-4}
$C_{27}H_{50}N_2O_4$	6.42×10^{-10}–3.29×10^{-7}	7.23×10^{-6}–1.95×10^{-3}
$C_{27}H_{50}N_2O_5$	3.11×10^{-11}–1.05×10^{-6}	7.23×10^{-6}–1.95×10^{-3}
$C_{27}H_{52}N_2O_3$	4.94×10^{-8}–2.76×10^{-6}	7.23×10^{-6}–1.95×10^{-3}
$C_{28}H_{52}N_2O_6$	1.14×10^{-14}–8.03×10^{-8}	2.81×10^{-6}–7.57×10^{-4}
$C_{28}H_{54}N_2O_6$	5.95×10^{-15}–1.03×10^{-7}	2.81×10^{-6}–7.57×10^{-4}
$C_{28}H_{56}N_2O_3$	6.09×10^{-8}–1.38×10^{-6}	2.81×10^{-6}–7.57×10^{-4}
$C_{28}H_{56}N_2O_6$	1.89×10^{-14}–5.88×10^{-9}	2.81×10^{-6}–7.57×10^{-4}
$C_{28}H_{58}N_2O_3$	3.18×10^{-8}	2.81×10^{-6}–4.66×10^{-6}
$C_{29}H_{56}N_2O_6$	2.30×10^{-15}–3.99×10^{-8}	1.09×10^{-6}–2.94×10^{-4}
$C_{29}H_{59}NO_7$	2.85×10^{-17}–6.47×10^{-16}	1.11×10^{-5}–2.94×10^{-4}
$C_{33}H_{59}NO_5$	1.05×10^{-12}–3.02×10^{-8}	2.49×10^{-7}–6.65×10^{-6}
$C_{34}H_{59}NO_6$	2.13×10^{-15}–1.38×10^{-9}	9.64×10^{-8}–2.57×10^{-6}
$C_{34}H_{66}N_2O_3$	1.15×10^{-11}–3.58×10^{-9}	9.45×10^{-9}–2.57×10^{-6}
$C_{34}H_{68}N_2O_3$	2.03×10^{-10}–4.61×10^{-9}	9.45×10^{-9}–2.57×10^{-6}
$C_{34}H_{68}N_2O_5$	3.75×10^{-15}–2.88×10^{-9}	9.45×10^{-9}–2.57×10^{-6}